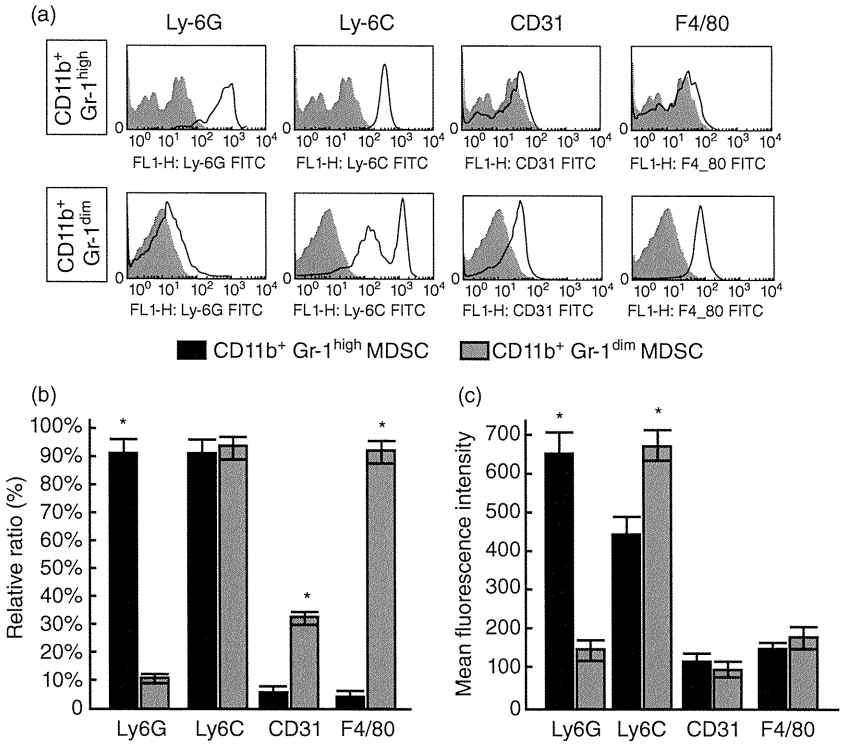

Fig. 2. Phenotypic analyses of myeloid-derived suppressor cells (MDSC) subtypes of normal mice liver. (a) Representative histograms of phenotypic profiles of $CD11b^+Gr1^{high}$ MDSC and $CD11b^+Gr1^{dim}$ MDSC. (b) Proportions of Ly6G, Ly6C, CD31 and F4/80 in $CD11b^+Gr1^{high}$ MDSC and $CD11b^+Gr1^{dim}$ MDSC of liver from normal mice. (c) Levels of expression of Ly6G, Ly6C, CD31 and F4/80 [shown by mean fluorescence intensity (MFI) on $CD11b^+Gr1^{high}$ MDSC and $CD11b^+Gr1^{dim}$ MDSC. * $P < 0{\cdot}05$, compared to other subtypes.

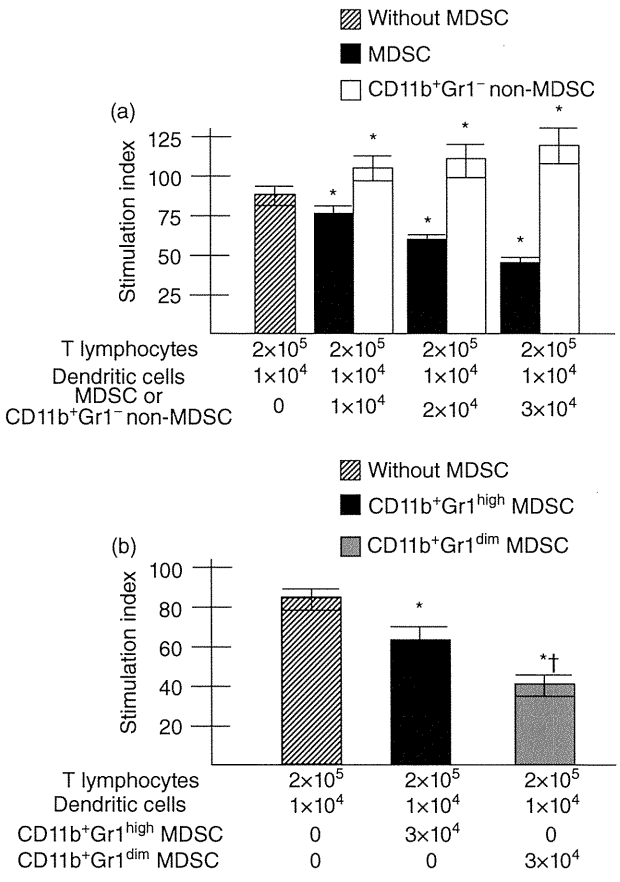

Fig. 3. (a) Suppression of T cells proliferation by liver myeloid-derived suppressor cells (MDSC), but not by liver non-MDSC. T cells (2×10^5) and dendritic cells (1×10^4) from spleen of normal mice were cultured in allogenic mixed leucocyte reaction (MLR). MDSC or $CD11b^+Gr^-$ non-MDSC were added to allogenic MLR, as mentioned. The levels of T cell proliferation are shown as the stimulation index (SI), as described in the Methods. The levels of SI in allogenic MLR without MDSC are shown as hatched bar and those in presence of MDSC and $CD11b^+Gr^-$ non-MDSC are shown as black bar and clear bar, respectively. Data of five separate experiments are shown, with means and standard deviations. *$P < 0{\cdot}05$ compared to levels of T cell proliferation in allogenic MLR without MDSC. (b) Increased T cell suppressive capacity of $CD11b^+Gr1^{dim}$ MDSC compared to $CD11b^+Gr1^{high}$ MDSC in allogenic MLR. The experimental conditions of allogenic MLR are similar to that described in Fig. 3a. *$P < 0{\cdot}05$ compared to levels of T cell proliferation in allogenic MLR without MDSC. †$P < 0{\cdot}05$ compared to levels of T cell proliferation in allogenic MLR containing $CD11b^+Gr1^{high}$ MDSC.

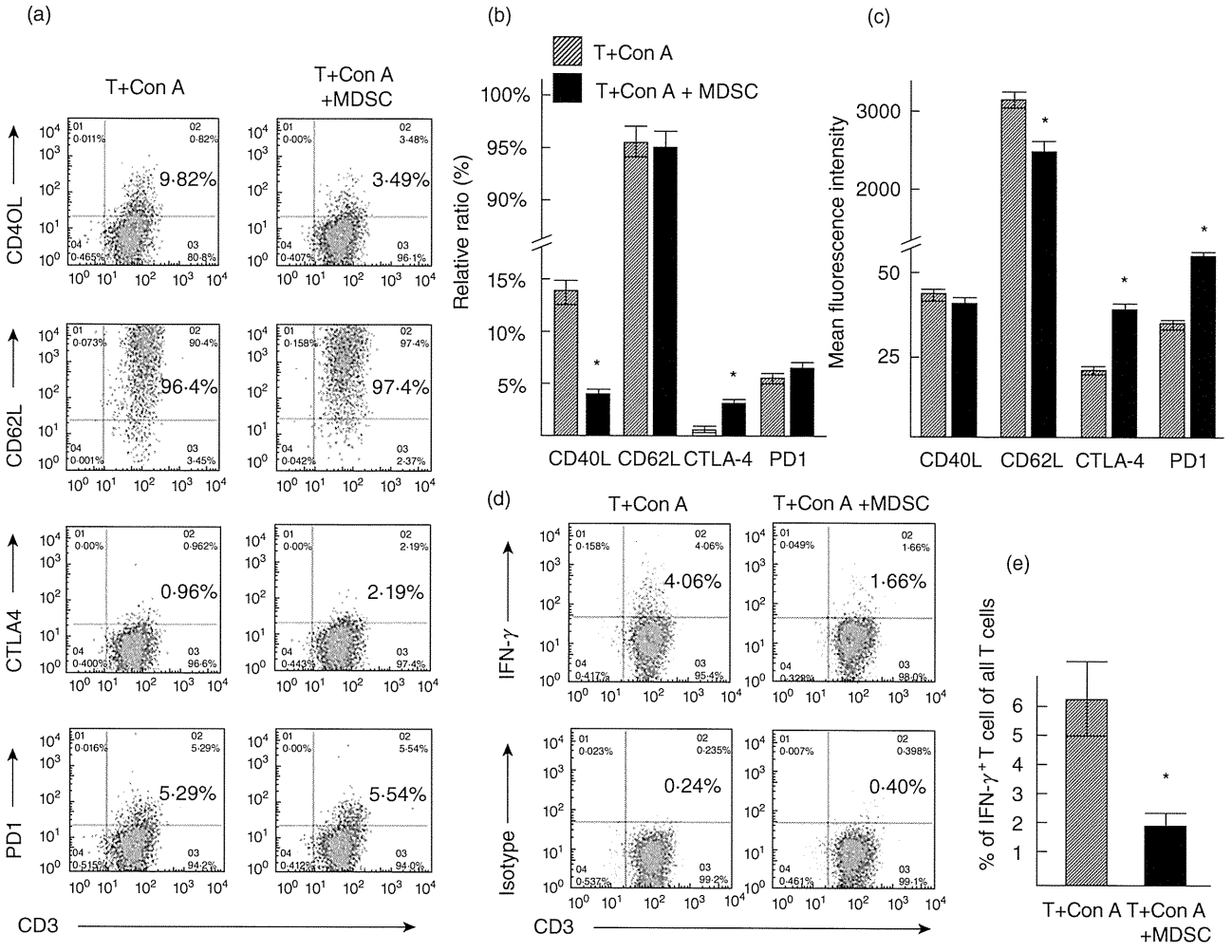

Fig. 4. (a) Representative dot-plots of CD40L, CD62L, CTLA-4 and PD1 antigens on T lymphocytes cultured without or with myeloid-derived suppressor cells (MDSC). (b) The ratio of T cells expressing CD40L, CD62L, CTLA-4 and PD1 antigens cultured without or with MDSC. (c) The levels of expression (shown by mean fluorescence intensity) of CD40L, CD62L, CTLA-4 and PD1 antigens cultured without or with MDSC. (d) A representative staining of intracellular interferon (IFN)-γ in T cells among all T cells cultured without or with MDSC. (e) Data of five separate experiments about intracellular IFN-γ production by T cells among all T cells are shown. $n = 5$, $^*P < 0{\cdot}05$, compared to without MDSC.

liver are regulated by several suppressor immunocytes, such as regulatory DC [18], regulatory NK cells [19] and regulatory T cells [20]. Interestingly, these suppressor cells of the liver also have immunogenic counterparts; immunogenic DC for regulatory DC, immunogenic T cells for regulatory T cells and immunogenic NK cells for regulatory NK cells. It seems that comprehensive functions of immunosuppressive immunocytes and immunogenic immunocytes maintain normal homeostasis under physiological conditions.

In this regard, there is a paucity of information about hepatic $CD11b^+$ myeloid cells and their functional implications. Generally, it is assumed that $CD11b^+$ myeloid cells are capable of producing inflammatory cytokines and play a role as immunogenic cells. Recently, it has been shown that MDSC, a subpopulation of $CD11b^+$ myeloid cells that express both CD11b and Gr1 antigens, are endowed with immunosuppressive properties in cancer patients and in mice models of different cancers [1,2,4,5]. However, there is a paucity of information about localization, frequencies and functions of MDSC in the normal liver.

The studies presented here showed that MDSC were present in the liver of normal mice and suppressed non-antigen-specific (Fig. 3) as well as antigen-specific T cell proliferation (Fig. 5). To be more confident about the immunosuppressive properties of liver MDSC, we compared the functional capacities of liver MDSC and non-MDSC myeloid cells of the liver (cells expressing $CD11b^+Gr1^-$) in the same run. The data showed conclusively that MDSC, but not other myeloid cells, were immunosuppressive (Fig. 3).

We detected two subtypes of MDSC in the liver on the basis of expression of Gr1 antigen. Further analyses revealed that these two subtypes showed significant differences regarding expressions of Ly-6G, Ly-6C, CD31 and F4/80

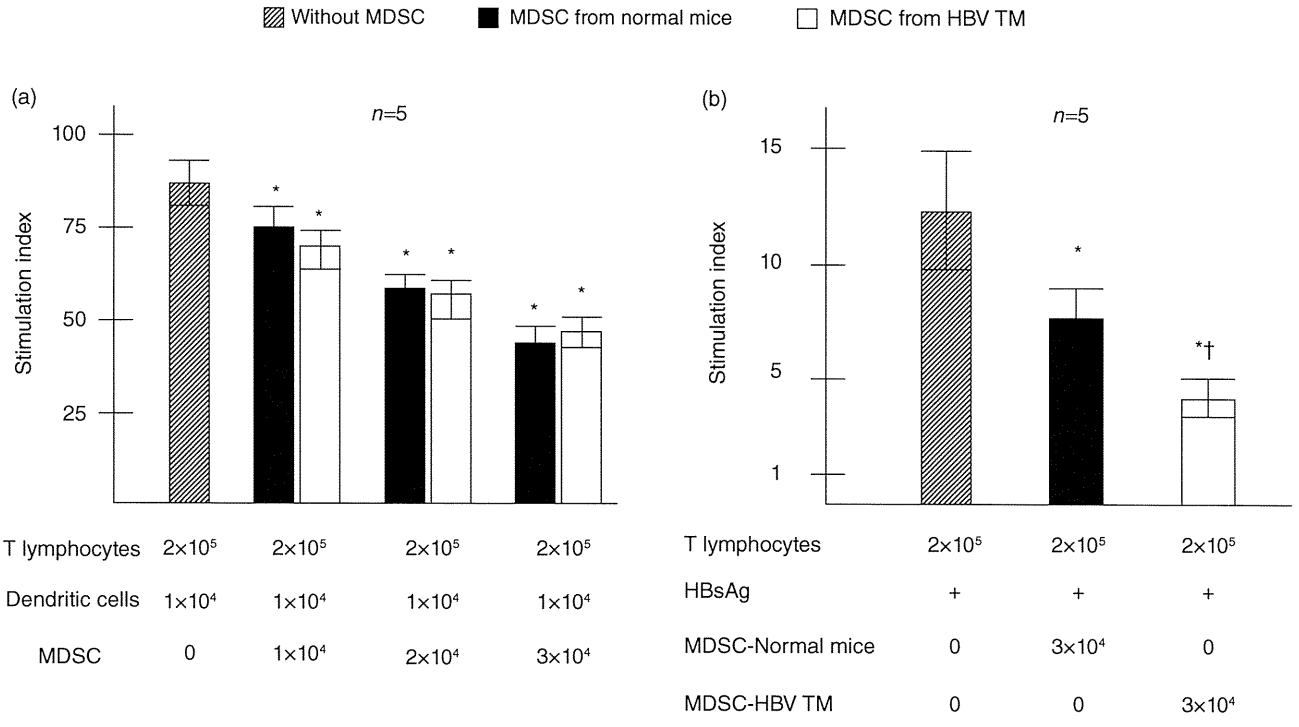

Fig. 5. T cell suppressive capacity of hepatitis B virus transgenic mice (HBV TM)-derived MDSC. (a) T cell suppression by HBV TM-derived MDSC in allogenic MLR. (b) Suppression of antigen-specific lymphocyte proliferation by liver MDSC. T cells (2×10^5) from hepatitis B surface antigen (HBsAg)-injected mice were cultured with or without HBsAg. MDSC from normal mice and HBV TM were added to the cultures. The levels of T cell proliferation are shown as the stimulation index (SI), as described in the Methods. The levels of SI in lymphocyte proliferation without MDSC are shown as hatched bar and those in presence of MDSC from normal mice and HBV TM are shown as black bar and clear bar, respectively. Data of five separate experiments are shown, with means and standard deviations. $*P < 0{\cdot}05$ compared to levels of HBsAg-specific lymphocyte proliferation without MDSC. $\dagger P < 0{\cdot}05$ compared to levels of T cell proliferation in HBsAg-specific lymphocyte proliferation containing normal mice-derived MDSC.

antigens (Fig. 2). In addition, the magnitudes of T cell suppressive capacities of $CD11b^+$ $Gr1^{dim}$ MDSC were significantly higher than $CD11b^+$ $Gr1^{high}$ MDSC, the clinical implications of which should be assessed in a future study. Although both subtypes are now regarded as MDSC, further studies would be required to gain more insight into their roles in hepatic immunity in normal as well as in pathological conditions.

Various tumour-derived factors as well as arginase, nitric oxide and reactive oxygen species play a role in MDSC accumulation and their immunosuppressive functions in cancers [7–10]. In addition, MDSC-mediated immunosuppression is mediated, at least in part, through the regulation of functions of NK cells and DC [21,22] in cancers. Using a model of Con-A-induced T cell proliferation, this study pointed that MDSC may have some effects on expression of T cell antigen (Fig. 4). However, this should be confirmed in other models of T cell proliferation, especially in antigen-specific T cell proliferation. Addition of MDSC in T cell cultures down-regulated production of IFN-γ in T cells (Fig. 4).

In addition to exploring the functional capacities of MDSC in normal mice liver, we also checked MDSC function in a pathological condition other than cancer. The proportions of MDSC in the liver were significantly higher in HBV TM compared with those in the liver of normal mice. MDSC from HBV TM suppressed T cell proliferation in allogenic MLR. In addition, MDSC from HBV TM revealed significantly increased the capacity to suppress proliferation of HBsAg-specific lymphocytes compared to normal mice-derived MDSC (Fig. 5).

Immunosuppressive activity of MDSC in HBV TM, especially suppression of antigen-specific T cell proliferation by MDSC, is worthy of further study because manipulation of MDSC may have therapeutic implications. It has been shown that treatment that reduces MDSC levels, such as antibody depletion of Gr1 cells, or treatments that down-regulate MDSC, such as chemotherapeutic drugs or retinoic agents, improve the efficacy of cancer vaccines or other immunotherapy *in vivo* [23–27]. At present, there is no curative therapy against chronic HBV infection [28]. Immune therapy has been accomplished in patients with chronic hepatitis B, but an effective immune therapeutic regimen has yet to be developed. The therapeutic effects of different agents that deplete MDSC in HBV TM remain to be elucidated for the development of novel therapeutic approaches against chronic HBV infection.

In conclusion, this is one of the first reports to show that MDSC are present in the liver of normal mice. In addition, these cells were shown to suppress T cell immunity. We also showed that in contrast to $CD11b^+$ $Gr1^{high}$ MDSC, $CD11b^+$ $Gr1^{dim}$ MDSC were significantly higher in the liver and had increased immunosuppressive functions. Furthermore, we provided credible evidence about a role of MDSC in chronic HBV infection. Further studies into liver MDSC and their subtypes would provide more insight into the maintenance of hepatic homeostasis in the normal liver and information about immunosuppression after infection with hepatotrophic viruses. Finally, it may be possible to develop novel therapeutic strategies against these diseases by targeting MDSC.

Acknowledgements

We thank the Integrated Center for Science, Shigenobu Station, Ehime University for animal management and cell sorting.

Disclosures

The authors declare that there are no conflicts of interest related to the publication of this manuscript.

References

1 Gabrilovich DI, Nagaraj S. Myeloid-derived suppressor cells as regulators of the immune system. Nat Rev Immunol 2009; **9**:162–74.

2 Pak AS, Wright MA, Matthews JP, Collins SL, Petruzzelli GJ, Young MR. Mechanisms of immune suppression in patients with head and neck cancer: presence of CD34-cells which suppress immune functions within cancers that secrete granulocyte–macrophage colony-stimulating factor. Clin Cancer Res 1995; **1**:95–103.

3 Young MR, Kolesiak K, Wright MA, Gabrilovich DI. Chemoattraction of femoral CD34-progenitor cells by tumor-derived vascular endothelial cell growth factor. Clin Exp Metastasis 1999; **17**:881–8.

4 Kusmartsev S, Nagaraj S, Gabrilovich DI. Tumor-associated CD8-T cell tolerance induced by bone marrow-derived immature myeloid cells. J Immunol 2005; **175**:4583–92.

5 Serafini P, Carbley R, Noonan KA, Tan G, Bronte V, Borrello I. High-dose granulocyte–macrophage colony-stimulating factor-producing vaccines impair the immune response through the recruitment of myeloid suppressor cells. Cancer Res 2004; **64**: 6337–43.

6 Sinha P, Okoro C, Foell D, Freeze HH, Ostrand-Rosenberg S, Srikrishna G. Proinflammatory S100 proteins regulate the accumulation of myeloid-derived suppressor cells. J Immunol 2008; **181**:4666–75.

7 Liu C, Yu S, Kappes J *et al.* Expansion of spleen myeloid suppressor cells represses NK cell cytotoxicity in tumor-bearing host. Blood 2007; **109**:4336–42.

8 Sinha P, Clements VK, Ostrand-Rosenberg S. Reduction of myeloid-derived suppressor cells and induction of M1 macrophages facilitate the rejection of established metastatic disease. J Immunol 2005; **174**:636–45.

9 Sinha P, Clements VK, Bunt SK, Albelda SM, Ostrand-Rosenberg S. Cross-talk between myeloid-derived suppressor cells and macrophages subverts tumor immunity toward a type 2 response. J Immunol 2007; **179**:977–83.

10 Huang B, Pan PY, Li Q *et al.* Gr-1+CD115+ immature myeloid suppressor cells mediate the development of tumor-induced T regulatory cells and T-cell anergy in tumor-bearing host. Cancer Res 2006; **66**:1123–31.

11 Mehal WZ, Azzaroli F, Crispe IN. Immunology of the healthy liver: old questions and new insights. Gastroenterology 2001; **120**:250–60.

12 Crispe IN, Dao T, Klugewitz K, Mehal WZ, Metz DP. The liver as a site of T-cell apoptosis: graveyard or killing field? Immunol Rev 2000; **174**:47–62.

13 Akbar SM, Onji M, Inaba K, Yamamura K-I OY. Low responsiveness of hepatitis B virus transgenic mice in antibody response to T-cell-dependent antigen: defect in antigen presenting activity of dendritic cells. Immunology 1993; **78**:468–75.

14 Araki K, Miyazaki J, Hino O *et al.* Expression and replication of hepatitis B virus genome in transgenic mice. Proc Natl Acad Sci USA 1989; **86**:207–11.

15 Hasebe A, Akbar SM, Furukawa S, Horiike N, Onji M. Impaired functional capacities of liver dendritic cells from murine hepatitis B virus (HBV) carriers. Clin Exp Immunol 2005; **139**:35–42.

16 Yoshida O, Akbar F, Miyake T *et al.* Impaired dendritic cell functions because of depletion of natural killer cells disrupt antigen-specific immune responses in mice. Clin Exp Immunol 2008; **152**:174–81.

17 Miyake T, Akbar SM, Yoshida O *et al.* Impaired dendritic cell functions disrupt antigen-specific adaptive immune responses in mice with nonalcoholic fatty liver disease. J Gastroenterol 2010; **45**: 859–67.

18 Steinman RM, Nussenzweig MC. Avoiding horror autotoxicus: the importance of dendritic cells in peripheral T cell tolerance. Proc Natl Acad Sci USA 2002; **99**:351–8.

19 Yoshida O, Akbar SM, Chen S *et al.* Regulatory natural killer cells in murine liver and their immunosuppressive capacity. Liver Int 2010; **30**:906–12.

20 Sakaguchi S, Sakaguchi N, Asano M, Itoh M, Toda M. Immunogenic self-tolerance maintained by activated T cells expressing IL-2 receptor alpha-chains (CD25). Breakdown of a single mechanism of self-tolerance causes various autoimmune diseases. J Immunol 1995; **155**:1151–64.

21 Hoechst B, Voigtlaender T, Ormandy L *et al.* Myeloid derived suppressor cells inhibit natural killer cells in patients with hepatocellular carcinoma via the NKp30 receptor. Hepatology 2009; **50**:799–807.

22 Cheng P, Corzo CA, Luetteke N *et al.* Inhibition of dendritic cell differentiation and accumulation of myeloid-derived suppressor cells in cancer is regulated by S100A9 protein. J Exp Med 2008; **205**:2235–49.

23 Ugel S, Delpozzo F, Desantis G *et al.* Therapeutic targeting of myeloid-derived suppressor cells. Curr Opin Pharmacol 2009; **9**:470–81.

24 Vincent J, Mignot G, Chalmin F *et al.* 5-Fluorouracil selectively kills tumor-associated myeloid-derived suppressor cells resulting in enhanced T cell-dependent antitumor immunity. Cancer Res 2010; **70**:3052–61.

25 Kusmartsev S, Cheng F, Yu B *et al.* All-trans-retinoic acid eliminates immature myeloid cells from tumor-bearing mice and improves the effect of vaccination. Cancer Res 2003; **63**:4441–9.
26 Pan PY, Wang GX, Yin B *et al.* Reversion of immune tolerance in advanced malignancy: modulation of myeloid-derived suppressor cell development by blockade of stem-cell factor function. Blood 2008; **111**:219–28.
27 Mirza N, Fishman M, Fricke I *et al.* All-trans-retinoic acid improves differentiation of myeloid cells and immune response in cancer patients. Cancer Res 2006; **66**:9299–307.
28 Shamliyan TA, MacDonald R, Shaukat A *et al.* Antiviral therapy for adults with chronic hepatitis B: a systemic review for a National Institute of Health consensus development conference. Ann Intern Med 2009; **150**:111–24.

EXPERIMENTAL CELL RESEARCH 317 (2011) 1851–1859

available at www.sciencedirect.com

ScienceDirect

www.elsevier.com/locate/yexcr

Research Article

ZNF689 suppresses apoptosis of hepatocellular carcinoma cells through the down-regulation of Bcl-2 family members

Shuichiro Shigematsu[a,b], *Shinji Fukuda*[b], *Hironao Nakayama*[b], *Hirofumi Inoue*[b,d], *Yoichi Hiasa*[a,c], *Morikazu Onji*[a], *Shigeki Higashiyama*[b,c,d,*]

[a] *Department of Gastroenterology and Metabology, Ehime University Graduate School of Medicine, Ehime, Japan*
[b] *Department of Biochemistry and Molecular Genetics, Ehime University Graduate School of Medicine, Ehime, Japan*
[c] *Department of Cell Growth and Tumor Regulation, Proteo-Medicine Research Center (ProMRES), Ehime, Japan*
[d] *Bioimaging Core Laboratory, Proteo-Medicine Research Center (ProMRES), Ehime, Japan*

ARTICLE INFORMATION

Article Chronology:
Received 18 January 2011
Revised version received 19 April 2011
Accepted 13 May 2011
Available online 20 May 2011

Keywords:
ZNF689
Hepatocellular carcinoma
Apoptosis
Zinc finger transcription factor

ABSTRACT

ZNF689, a C2H2-type of zinc finger transcription factor, was suggested to play a key role in hepatocarcinogenesis. However, none of the target genes or potential roles of ZNF689 in hepatocellular carcinoma (HCC) have been elucidated. Here, we investigated the role of ZNF689 in HCC cell lines focusing on cell viability and apoptosis. We found that the knockdown of ZNF689 by its specific siRNA decreased cell viability of Huh7. Cell cycle analysis revealed that the ZNF689 knockdown increased the proportion of the sub-G1 population, accompanied by an increase of annexin V- and TUNEL-positive cells. Western blot analysis revealed that ZNF689 knockdown induced the expression of pro-apoptotic factors of Bcl-2 family, Bax, Bak and jBid. There was a correlation between the expression of ZNF689 and an anticancer drug 5-fluorouracil (5-FU) resistance of HCC cells. *In vivo*, ZNF689 siRNA reduced tumor viability in HepG2-bearing mice with statistical significance. Furthermore, immunohistochemical analysis demonstrated that nuclei of a significant portion of human HCC surgical specimens were positive for ZNF689. Taken together, our results indicate that ZNF689 blocks pro-apoptotic signaling by suppressing the Bak/Bax/Bid pathway, resulting in the progression of liver cancer and resistance to 5-FU. ZNF689 may be a promising chemotherapeutic target against liver cancer.

Introduction

Hepatocellular carcinoma (HCC) is one of the most common cancers worldwide [1]. Surgical resection, liver transplantation, and percutaneous ablation offer the best prognosis for long-term survival [2]. Unfortunately, most HCC patients are diagnosed at advanced stages, when they are not suitable for curative operations due to extensive disease or severe liver dysfunction [3]. Although chemotherapy is an alternative choice as a multimodal treatment for advanced HCC, there is no generally accepted standard chemotherapy regimen, because of the low sensitivity and/or drug resistance to anticancer agents.

A crucial step to establish new strategies for cancer treatment is the identification of molecules that drive enhanced proliferation accompanied by a reduced rate of cell death. A common finding in chronic inflammatory liver disease and in HCC is the activation of growth factor expression and signaling. Among the relevant growth factors and their receptors to hepatocarcinogenesis are epidermal growth factor (EGF) family members such as heparin-binding EGF (HB-EGF), amphiregulin and transforming

* *Corresponding author at:* Department of Biochemistry and Molecular Genetics, Ehime University Graduate School of Medicine, Shitsukawa, Toon, Ehime 791-0295, Japan. Fax: +81 89 960 5256.
E-mail address: shigeki@m.ehime-u.ac.jp (S. Higashiyama).

0014-4827/$ – see front matter © 2011 Elsevier Inc. All rights reserved.
doi:10.1016/j.yexcr.2011.05.012

growth factor-α (TGF-α), and the EGF receptor (EGFR) [4]. We previously reported the enhanced expression of HB-EGF in HCC [5]. Recently, we identified promyelocytic leukemia zinc finger protein (PLZF) and its related factor B-cell leukemia 6 (Bcl6) as binding partners of C-terminal domain of membrane-anchored HB-EGF (proHB-EGF), which regulate multiple factors essential for cell cycle progression such as c-Myc, cyclin A, and cyclin D [6–8]. Both PLZF and Bcl6 contain tandem repeats of the Krüppel-like C2H2-type zinc finger domain at their carboxyl-terminal regions. A comprehensive oncogenomic database for HCC, OncoDB.HCC [9], indicates that more than 10 C2H2-type zinc finger proteins are expressed, some of which might play key roles in hepatocarcinogenesis.

In this study, we focused on one of these putative transcription factors, ZNF689, which is a recently identified C2H2-type of Krüppel-associated box (KRAB)-zinc finger protein specifically expressed in HCC but not in noncancerous liver tissues [10]. The previous study showed that over-expression of ZNF689 conferred anchorage-independent growth of NIH3T3 cells, and that knockdown of ZNF689 in HCC resulted in their growth inhibition [10], suggesting a key role in hepatocarcinogenesis. However, the molecular mechanism of ZNF689 function still remains unknown. Here we show that ZNF689 suppressed apoptotic signaling through down-regulation of apoptosis-promoting factors Bak/Bax/Bid, and suggest that molecular targeting of ZNF689-mediated anti-apoptotic effects may be an effective therapeutic strategy for HCC treatment.

Materials and methods

Cell culture

Huh7, HepG2, and Hep3B were obtained from the Health Science Research Resources Bank (HSRRB, Osaka, Japan) and cultured in Dulbecco's modified Eagle's medium supplemented with 10% fetal bovine serum, 100 units/ml penicillin and 10 μg/ml streptomycin in a humidified incubator with 5% CO_2 at 37 °C. 5-FU was purchased from Wako Pure Chemical Industries (Osaka, Japan). Nutlin-3 was purchased from Cayman Chemical (Ann Arbor, MI, USA).

Plasmid construction

Total RNA of Huh7 was extracted by TRIzol reagent (Invitrogen, Carlsbad, CA, USA), and used for the amplification of ZNF689 cDNA by the SuperScript RT III enzyme (Invitrogen). The entire coding region of ZNF689 was cloned into the expression vector pME18S-FLAG-NT. Lentiviruses used in this study were constructed by inserting cDNAs encoding ZNF689 or the stable luciferase green (SLG) from pSLG HSVTK control (TOYOBO, Osaka, Japan) into lentiviral expression vectors CSII-EF-MCS-IRES2-Venus and CSII-CMV-MCS-IRES2-Bsd (kindly provided by Dr. Miyoshi, RIKEN Bioresouce Center, Tsukuba, Japan).

qPCR analysis

For the expression profiling of apoptosis-related genes, RT2 Profiler PCR Array Human apoptosis (SABiosciences, Frederick, MD, USA) was used. qPCR was performed with the POWER SYBR Green PCR Master Mix and a 7300 Real-time PCR System (Applied Biosystems, Foster City, CA, USA) according to the manufacturer's protocol. Primer sequences used for qPCR were as follows:

GAPDH forward, 5′-TGCACCACCAACTGCTTAGC-3′;
GAPDH reverse, 5′-GGCATGGACTGTGGTCATGAG-3′;
ZNF689 forward, 5′-TGGAACGAAACACCGATGACT-3′;
ZNF689 reverse, 5′-CCATTCTTCTTTCTGGTTCTGCT-3′;
Bak forward, 5′-GAACAGGAGGCTGAAGGGGT-3′;
Bak reverse, 5′-TCAGGCCATGCTGGTAGACG-3′;
Bax forward, 5′-GCTGTTGGGCTGGATCCAAG-3′;
Bax reverse, 5′-TCAGCCCATCTTCTTCCAGA-3′.

Cell proliferation assay

Cell viability was quantified by a WST-1 colorimetric assay (Roche Applied Science, Basel, Switzerland). Briefly, 2×10^3 cells were seeded in 96-well plates. At each time point, cells were treated with WST-1 reagent and incubated for 120 min. The absorbance at 450 nm was recorded.

Gene silencing with small interfering RNA (siRNA)

siRNA cocktail against ZNF689 was purchased from B-Bridge International (Cupertino, CA, USA). HCC cells were transfected with the control or ZNF689 siRNA (5 nM for Huh7 and 20 nM for HepG2 and Hep3B) by Lipofectamine RNAiMax (Invitrogen) according to the instruction manual. The knockdown efficiency was validated by qPCR and Western blot analyses.

Detection of cell death

Early apoptosis was quantified using an Annexin V-FITC kit (Beckman Coulter, Brea, CA, USA) and 7-amino-actinomycin D (7-AAD) according to the manufacturer's protocol. Cells stained with annexin V-FITC and 7-AAD were analyzed by flow cytometry with a FACSCalibur (BD Bioscience, San Diego, CA, USA). Late apoptosis was evaluated by TUNEL Assay using an ApopTag fluorescein *in situ* apoptosis detection kit (Chemicon International, Inc., Temecula, CA, USA) according to the manufacturer's protocol.

Antibodies

Affinity-purified rabbit polyclonal antibody against synthetic peptides corresponding to the linker region of ZNF689 (residues 127–139) was obtained from Sigma-Aldrich (St. Louis, MO, USA). For the detection of Bcl-2 family proteins, a Pro-Apoptosis Bcl-2 Family Antibody Sampler Kit (Cell Signaling Technology, Beverly, MA, USA) and a rabbit anti-Bak antibody (Y164; Abcam, Cambridge, UK) were used. Other antibodies used were as follows: anti-FLAG (M2, Sigma) anti-β-actin (AC-15, Sigma), Anti-nucleolin (3G4B20, Millipore, Billerica, MA, USA), anti-JNK and anti-phospho-JNK (Cell Signaling Technology).

Luciferase reporter assays

Huh7 cells cultured in 12-well plates were transfected with the Bak promoter-luciferase reporter (kindly provided by Dr. Licht, Northwestern University Feinberg School of Medicine) and the internal control, pRL-CMV (Promega, Madison, WI, USA), together with or without FLAG-ZNF689-pME18S using Lipofectamine 2000 (Invitrogen). Cells were harvested at 24 h post-transfection, and

the luciferase activity was measured by a Dual-Luciferase Reporter Assay System and GLOMAX 96 microplate luminometer (Promega) according to the manufacturer's protocol.

In vivo luminescence imaging assay

HepG2 were stably labeled with green-emitting luciferases [stable luciferase green (SLG)] by a lentiviral expression system. One million SLG-expressing HepG2 cells were subcutaneously inoculated into 5-week-old female Balb/c nude mice. After 3 weeks, the tumor-bearing nude mice were treated with ZNF689 siRNA cocktail or control siRNA mixed with atelocollagen (KOKEN, Tokyo, Japan) according to the manufacturer's protocol. D-luciferin was intraperitoneally injected at the indicated day and the transplanted cells in the mice were detected by an *in vivo* bioluminescence method using AEQUORIA-2D (Hamamatsu Photonics, Hamamatsu, Japan). All mice received standard care, and our study protocol was approved by the Ethics Committee of the Graduate School of Medicine, Ehime University, Japan.

Human liver specimens

Paraffin-embedded formalin fixed human liver tissues were obtained by surgical resection of 12 cases of HCCs. Sections were 4–6 μm thick. The Ethics Committee of Ehime University approved the study protocol. Written informed consent was obtained prior to enrolment in accordance with the principles of the Declaration of Helsinki (Approval No. 0809006).

Results

Knockdown of the ZNF689 gene induced apoptosis in HCC cells in a caspase-dependent manner

To examine the role of ZNF689 in HCC cell lines, we first assessed the viability of Huh7 by the siRNA-mediated knockdown of ZNF689. Down-regulation of ZNF689 expression by siRNA was validated by quantitative-polymerase chain reaction (qPCR) and

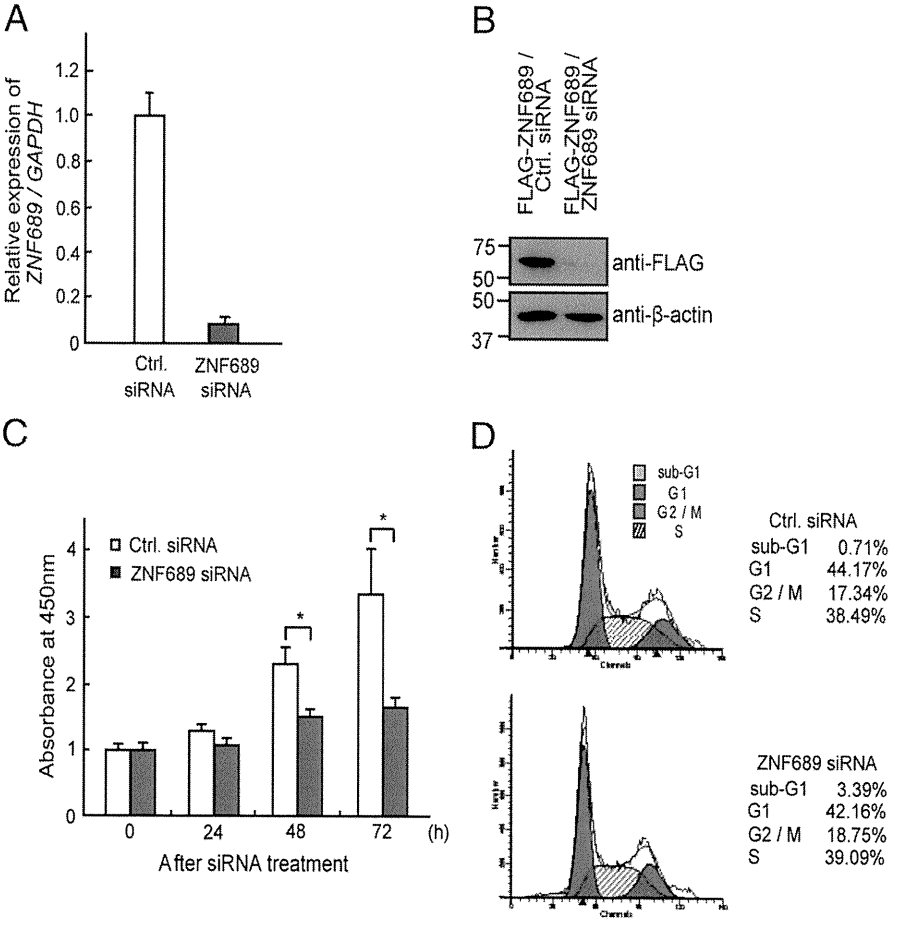

Fig. 1 – Effects of the knockdown of ZNF689 on the cell viability and cell cycle of the HCC cell line, Huh7. A. Knockdown efficiency of ZNF689 by its specific siRNA. Huh7 was transfected with either control (white bars) or ZNF689-specific (gray bars) siRNA. The expression of ZNF689 mRNA was quantified by qPCR and normalized by the expression of GAPDH as the internal control. B. Effects of siRNA against ZNF689 protein was examined by Western blot analysis. After 2 days of FLAG-ZNF689 transfection, Huh7 was further transfected with either control or ZNF689 siRNA. FLAG-ZNF689 was detected by using anti-FLAG antibody. C. Viability of control siRNA- and ZNF689 siRNA-transfected cells. Huh7 was transfected with either the control (white bars) or ZNF689-specific (gray bars) siRNA, and cell viability was measured by WST-1 assay at the indicated time points. The asterisk indicates $p < 0.05$. D. FACS analysis of Huh7 transfected with either the control (upper panel) or ZNF689 (lower panel) siRNA. The siRNA-transfected cells were stained with propidium iodide and the cell cycle was examined by FACS analysis.

Western blot analyses (Figs. 1A and B). We found that the viability of Huh7 decreased significantly 48 to 72 h after the transfection of ZNF689 siRNA (Fig. 1C). We further stained Huh7 with propidium iodide (PI) and analyzed the cell cycle stages by FACS 72 h after siRNA transfection. Although the overall cell cycle was not altered between the control and the ZNF689 siRNA-transfected cells, the proportion of the sub-G1 population was different, showing 3.39% and 0.71% in ZNF689 knockdown cells and control cells, respectively (Fig. 1D). Forty-eight hours after transfection, we observed an increased number of annexin V-positive cells in ZNF689 knocked-down cells (Fig. 2A). Furthermore, TUNEL-positive cells also increased at 72–96 h after the transfection (Figs. 2B and C). Thus, we assumed that the increase of the sub-G1 population caused by ZNF689 siRNA was due to the apoptosis of Huh7 cells.

To examine whether ZNF689 knockdown-induced cell death was caused by caspase-dependent apoptosis [11], Huh7 was transfected with siRNA and cultured in the presence of a pan-caspase inhibitor, Z-VAD-fmk. Z-VAD-fmk significantly suppressed the appearance of TUNEL-positive cells induced by ZNF689 siRNA (Figs. 3A and B). Furthermore, as judged by a tetrazolium salt (WST-1) assay in Huh7 cells, cell viability was partially, but significantly, restored by the use of Z-VAD-fmk (Fig. 3C), indicating that the caspase-dependent pathway is involved in ZNF689 knockdown-induced apoptosis.

We also confirmed the effect of ZNF689 siRNA on other HCC cell lines HepG2 and Hep3B cells. ZNF689 siRNA effectively knocked down ZNF689 mRNA in HepG2 and Hep3B cells, and increased the number of TUNEL-positive cells in both of the cells to a similar extent as that in Huh7 cells, which were significantly blocked with Z-VAD-fmk (Figs. S1A–C).

Taken together, these data suggest that the role of ZNF689 is to suppress the apoptosis of HCC cells through regulation of the caspase-dependent signaling pathway.

ZNF689 negatively regulates Bcl-2 family pro-apoptotic factors

It is known that caspase-dependent apoptosis occurs through two major pathways. One is the extrinsic pathway which involves the stimulation of members of the TNF, Fas or TRAIL receptors. The other is the intrinsic pathway in which a range of BH3-only proteins act as sentinels for cell stress [11]. The BH3-only proteins induce apoptosis by increasing mitochondrial outer membrane permeability, resulting in the release of cytochrome c [12]. In order to analyze the function of ZNF689 in these caspase-dependent pathways, we first compared gene expression profiles of apoptosis-related genes between the ZNF689 siRNA- and control siRNA-transfected Huh7 cells using real-time PCR arrays. Since ZNF689 is identified as a member of the KRAB-zinc finger family of transcriptional repressors, we especially focused on pro-apoptotic genes that were suppressed under the steady-state and up-regulated by siRNA-mediated knockdown. qPCR analysis revealed that ZNF689 siRNA up-regulated the expression of the pro-apoptotic genes Bak and Bax in comparison with the control siRNA in Huh7 (Figs. 4A and B). We also examined the effects of ZNF689 siRNA on the expression of the pro-apoptotic genes Bak and Bax in HepG2 and Hep3B cells. After the transfection of ZNF689 siRNA, Bak mRNA increased with statistical significance in both of the cells, while Bax mRNA increased with statistical significance in HepG2 (Figs. S1D and E).

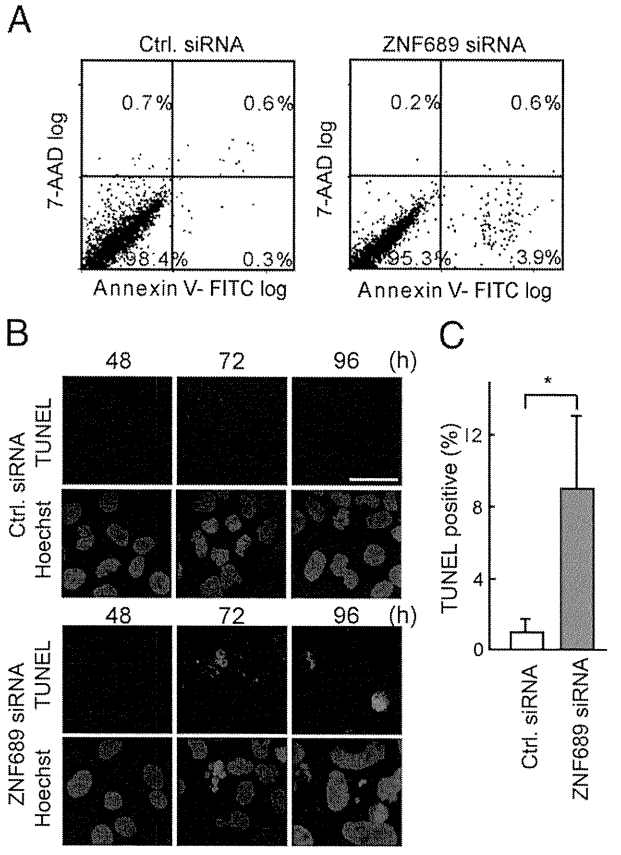

Fig. 2 – Knockdown of the ZNF689 expression induces apoptosis of Huh7. A. Early apoptosis of siRNA-treated Huh7. After the transfection of siRNA, cells were stained with Annexin V-FITC and 7-AAD, and analyzed by FACS. B. Late apoptosis of siRNA-treated Huh7. After the transfection of siRNA, TUNEL assay was performed at the indicated points. Nuclei were stained with Hoechst33342. Scale bar, 10 μm. C. The ratio of TUNEL-positive cells of control and ZNF689 siRNA-treated cells. TUNEL-positive cells shown in B were quantified. The asterisk indicates statistical significance ($p<0.05$).

Furthermore, we comprehensively examined the expression of pro-apoptotic Bcl-2 family proteins by Western blot analysis, and found the up-regulation of Bak and Bax proteins (Fig. 4C). To examine the activity of ZNF689 as a transcriptional repressor, we performed a luciferase assay using the Bak promoter [13], and found that ZNF689 significantly suppressed the promoter activity of the Bak gene (Fig. 4D). In addition, unexpectedly, jBid, one of the activated forms of Bid, was detected in ZNF689 siRNA-transfected Huh7 cells (Fig. 4C). Although the protease responsible for the processing of Bid has not been identified, it has been shown that jBid is generated by the JNK-dependent pathway [14]. We therefore assessed the activation of JNK, and found that the phosphorylated form of JNK increased in Huh7 cells transfected with ZNF689 siRNA (Fig. 4E). Furthermore, exposure of Huh7 to an apoptosis inducer, Nutlin-3, enhanced the extent of ZNF689 knockdown-mediated apoptosis, confirming that ZNF689 actually upregulates the expression of pro-apoptotic factors (Fig. 4F).

These results suggest that ZNF689 inhibits apoptosis through suppression of the expression of Bak/Bax and the appearance of

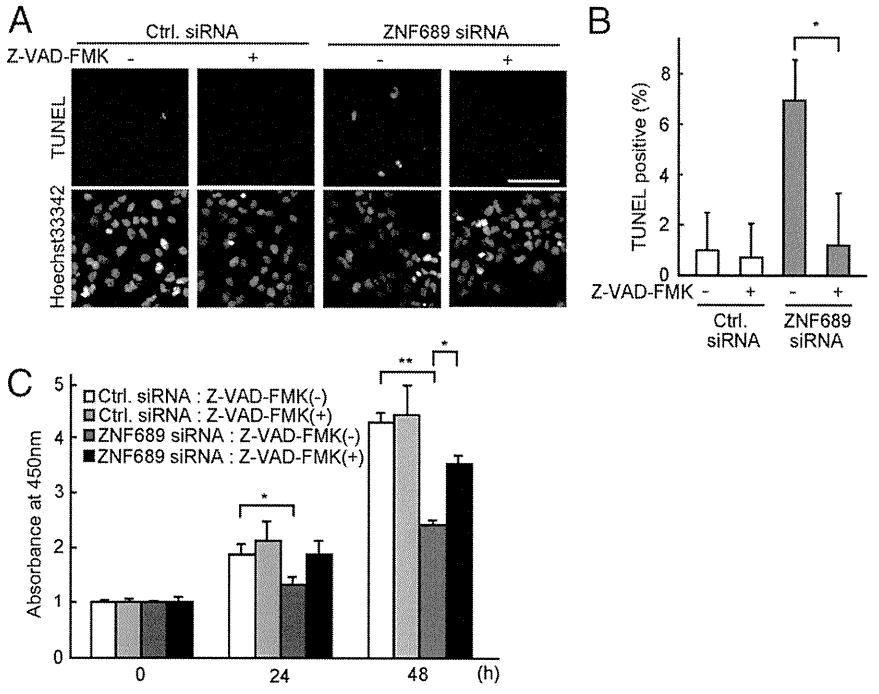

Fig. 3 – Pan-caspase inhibitor restores ZNF689-regulated cell death. A. Effects of the knockdown of ZNF689 and the Z-VAD-fmk treatment on Huh7. Control or ZNF689 siRNA-transfected Huh7 was treated with Z-VAD-FMK (20 nM). After 24 h incubation, apoptotic cells were detected by TUNEL assay. Nuclei were stained with Hoechst33342. Scale bar, 100 μm. B. The ratio of TUNEL-positive cells in A was quantified. The asterisk indicates $p < 0.05$. C. Cell viability of control or ZNF689 siRNA-transfected cells in the presence of Z-VAD-fmk. WST-1 assay was performed at the indicated time points. The asterisk indicates $p < 0.05$. Two asterisks indicate $p < 0.01$.

jBid. In the case of Bak regulation, ZNF 689 acts on the Bak promoter and represses its expression at the transcriptional level.

Correlation between the expression of ZNF689 and 5-FU resistance of HCC cells

Furthermore, we examined whether ZNF689 has a possible role in the anticancer drug resistance of HCC cells or not. We cultured Huh7 cells in the presence or absence of 5-fluorouracil (5-FU), commonly used for HCC chemotherapy. We analyzed the expression level of ZNF689 mRNA 1 week after the 5-FU addition when an arrest of cell proliferation was observed (Fig. 5A). Total RNA isolated from surviving Huh7 was examined by qPCR analysis, revealing an approximately three-fold increase of ZNF689 mRNA expression within 2 weeks of incubation (Fig. 5A). The up-regulation of ZNF689 mRNA was also observed in 5-FU-treated HepG2 and Hep3B to a different extent (Fig. S1F).

To examine the role of ZNF689 in 5-FU resistance of HCC, we knocked down the expression of ZNF689, and found that the viability of Huh7 in the presence of 5-FU decreased significantly as assessed by the WST-1 assay (Fig. 5B). The half maximal effective concentration (EC_{50}) value of 5-FU was 2.45 ± 0.42 μg/ml in control siRNA-transfected cells and 0.84 ± 0.55 μg/ml in ZNF689 siRNA-transfected cells ($p < 0.05$) (data not shown). Conversely, the EC_{50} value of 5-FU increased when ZNF689 was 5.46 ± 0.82 μg/ml in the control cells and 8.08 ± 1.30 μg/μl in ZNF689-overexpressed cells ($p < 0.05$) (data not shown).

Although the precise molecular mechanism underlying the increase of ZNF689 expression after the 5-FU treatment is unknown, we speculate that (1) 5-FU directly affects and upregulates the expression of ZNF689 gene, or (2) the 5-FU-resistant population in HCCs expresses higher amounts of ZNF689 than the 5-FU-sensitive population. These results suggested a correlation between the expression level of ZNF689 and 5-FU resistance in HCC cells, and implied that ZNF689 might have protective activity against anticancer agents.

Physiological role of ZNF689 in HCC-transplanted mice and human hepatocellular carcinoma surgical specimens

To understand the physiological role of ZNF689 *in vivo*, Huh7 and HepG2 cells stably labeled with a luciferase reporter were established and subcutaneously inoculated into nude mice. After 3 weeks, we detected tumor mass of HepG2, but not Huh7, by bioluminescence imaging. We then treated the HepG2 tumor-bearing nude mice with either ZNF689 siRNA or control siRNA (Fig. 6A). Under the experimental conditions we used, bioluminescent signals were significantly suppressed by ZNF689 siRNA compared with the control siRNA (Fig. 6B). These results suggest that ZNF689 affects the cell viability of HCC in transplanted mice as well as cultured HCC.

Finally, we raised polyclonal antibodies against a linker peptide of ZNF689 (amino acids 127–139). Although endogenous ZNF689 in Huh7 and HepG2 was undetectable by Western blot analysis using our anti-ZNF689 antibody, this antibody specifically recognized exogenously expressed ZNF689 tagged with a FLAG epitope as a single band (Fig. 6C). We immunostained FLAG-ZNF689 in Huh7 cells, and found that the FLAG-ZNF689 protein colocalized

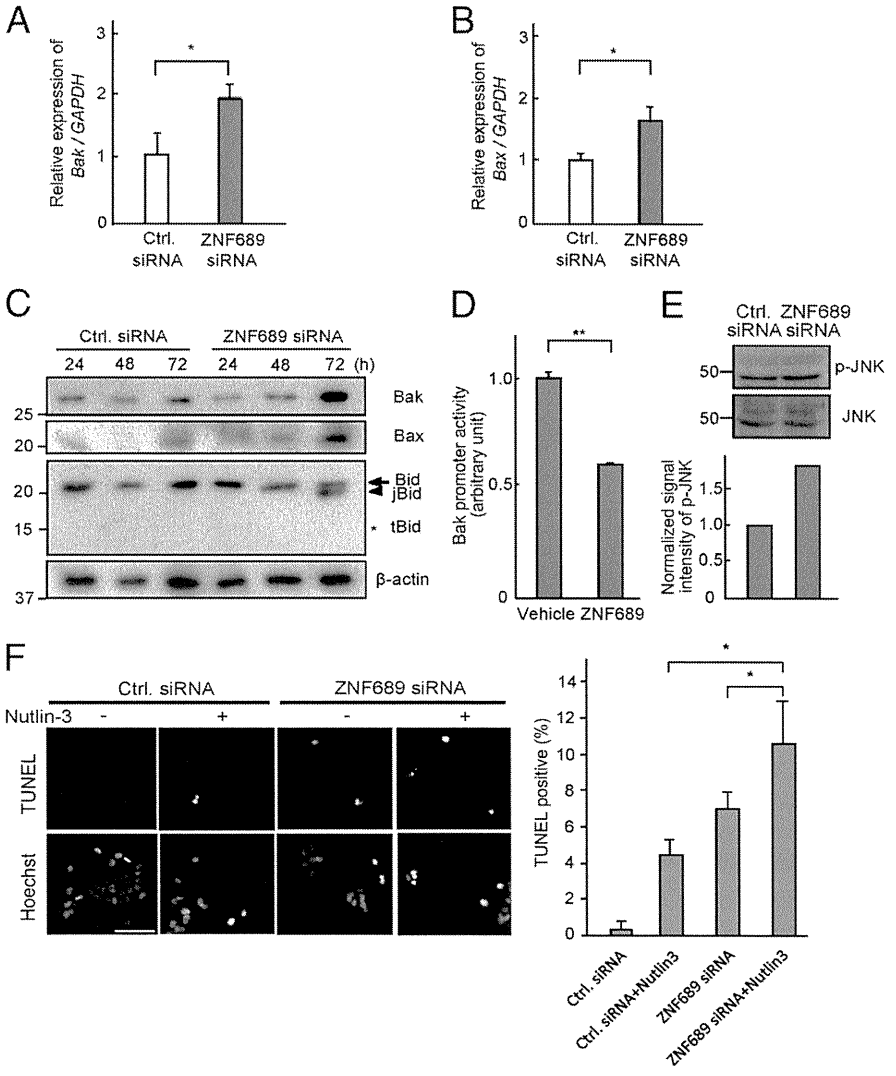

Fig. 4 – ZNF689 suppresses apoptosis through the negative regulation of apoptosis-promoting proteins. A. Upregulation of Bak mRNA expression by the knockdown of ZNF689. Total RNAs were isolated from Huh7 72 h after the transfection of either control (white bars) or ZNF689-specific (gray bars) siRNAs. The expression of Bak mRNA was quantified by qPCR and normalized by the expression of GAPDH as the internal control. B. The expression of Bax mRNA was quantified and normalized as in (A). C. Expression of Bcl-2 members of pro-apoptotic factors. Huh7 was transfected with either the control or ZNF689 siRNA, and cell lysates were prepared after the indicated time points. The expression of Bak, Bax, and Bid was examined by Western blot analysis. Full-length Bid and jBid are indicated by arrow and arrowhead, respectively. Asterisk indicates the molecular weight of tBid. β-actin was used as a loading control. D. ZNF689 suppresses the activation of Bak promoter activity. Huh7 cells were transfected with the Bak promoter-luciferase reporter plasmid and the internal control plasmid, together with or without the ZNF689-expression plasmid. After 24 h incubation, luciferase activity was measured. Two asterisks indicate $p < 0.01$. E. Phosphorylation of JNK in control or ZNF689 siRNA-treated Huh7. Band intensity of phosphorylated JNK was normalized by that of total JNK. F. Nutlin-3 enhanced ZNF689 knockdown-induced apoptosis. Control or ZNF689 siRNA-transfected Huh7 was treated with Nutlin-3 (2.5 μM). After 24 h incubation, apoptotic cells were detected by TUNEL assay. Nuclei were stained with Hoechst33342. TUNEL-positive cells in control and ZNF689 siRNA-treated cells were quantified and shown in right. Scale bar: 100 μm. The asterisk indicates statistical significance ($P < 0.05$).

with nucleolin, a nucleolus protein previously identified as a binding protein of ZNF689 (Fig. 6C). Immunohistochemical analysis using this antibody demonstrated that nuclei positive for ZNF689 were on the tumor margin or daughter nodules where cancer proliferates rapidly (Fig. 6D). In total, 25% of human HCC surgical specimens (4 of 12 cases) were positive for nuclear ZNF689.

Discussion

The development of novel HCC therapies requires understanding the molecules involved in hepatocarcinogenesis and the design of effective agents against responsible factors. The gene encoding ZNF689 was identified as up-regulated by a cDNA microarray analysis

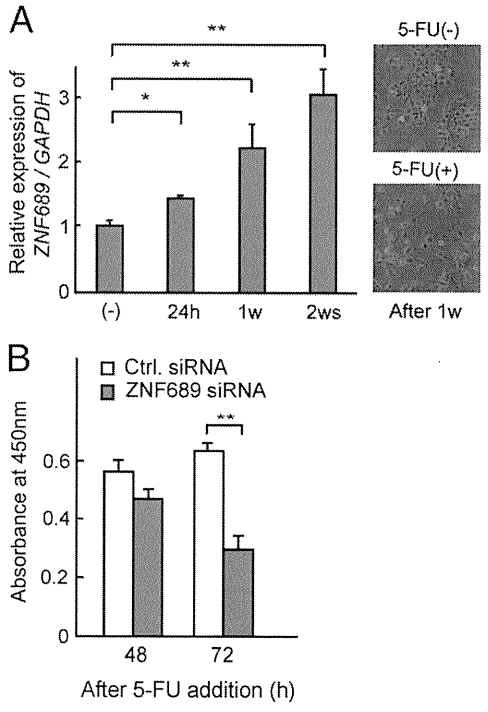

Fig. 5 – Correlation between the expression of ZNF689 and the 5-FU resistance. A. Time-course of ZNF689 mRNA levels in Huh7 following the 5-FU treatment (2 μg/ml). Total RNA of Huh7 was isolated after the 5-FU treatment at the indicated time points. The expression of ZNF689 mRNA was quantified by qPCR using GAPDH as the internal control. Right panels show bright field images of untreated and 5-FU-treated Huh7 after 1 week. B. Viability of control and ZNF689 siRNA-transfected cells in the presence of 5-FU. siRNA-transfected cells were cultured in the presence of 5-FU, and cell viability was measured by WST-1 assay. Two asterisks indicate $p < 0.01$.

of 20 human HCC tissues (termed as transcription-involved protein up-regulated in HCC: TIPUH1) [10]. Its protein, ZNF689, is a potential candidate for understanding the molecular mechanisms of hepatocarcinogenesis, as well as for diagnosis and therapy of HCC. Functional assessment of ZNF689 has primarily revealed that it has oncogenic activity in colony-formation assays in soft agar, and that it interacts with TIF1β, hnRNPU, hnRNPF, and nucleolin [10]. TIF1β is a transcriptional corepressor that recruits the histone deacetylase (HDAC) complex to DNA [15], and hnRNPU, hnRNPF, and nucleolin are all involved in mRNA or rRNA processing [16,17], suggesting that ZNF689 might regulate transcription repression and/or modification of RNA processing of genes essential for cell growth control [10]. However, none of the target genes or potential roles of ZNF689 have been elucidated to date.

In the present study, we characterized ZNF689 as an anti-apoptotic factor that modulates the apoptotic signaling cascade involving the Bcl-2 family of pro-apoptotic factors. Bak and Bax, members of the Bcl-2 family, are indispensable for apoptosis via the mitochondrial pathway, and apoptotic resistance is observed in Bak/Bax double knockout mice [18,19]. In a luciferase assay, ZNF689 suppressed the activation of the Bak promoter (Fig. 4D). Since ZNF689 has a transcriptional repression module, the KRAB domain [20], at its N-terminus, it is conceivable that ZNF689-mediated transcriptional repression is caused by its binding partner, TIF1β, and the recruitment of HDAC to the promoter region of the Bak gene. On the other hand, it is well known that another Bcl-2 member, Bid, is cleaved by caspase 8 for the generation of a 15-kDa protein, tBid [21], which drives the insertion of Bax into the membrane bilayer and oligomerization of Bax/Bak [12,22]. Treatment of Huh7 with ZNF689 siRNA generated a specific Bid antibody-reactive product migrating below the full-length Bid. Unexpectedly, it differed from tBid as judged from the molecular weight, and instead corresponded to a previously reported form of Bid, jBid. To date, only a single report is available for jBid, underscoring the lack of information on how jBid is processed from Bid [14]. Since we observed an increase of phosphorylated JNK in ZNF689 knockdown cells, ZNF689 might act on regulatory factor(s) upstream of JNK through transcriptional regulation. Further analysis of ZNF689 is necessary to elucidate the protease(s) activated by phosphorylated JNK, and the details of the unidentified component of the Bid-mediated pro-apoptotic pathway.

Accumulated evidence suggests an association between quantitative and qualitative defects in ribosome biogenesis and neoplastic transformation [23]. Up-regulation of hepatocyte ribosome biogenesis is consistently associated with later onset of HCC [24,25]. There is now evidence that proto-oncogene c-Myc binds to human ribosomal DNA and enhances RNA polymerase I transcriptional activity [26,27]. Since immunocytochemistry revealed that ZNF689 is localized in the nucleolus, and co-localizes with nucleolin, a ubiquitous eukaryotic protein essential for pre-ribosome assembly (Fig. 6C), up-regulated expression of ZNF689 may contribute to ribosome biogenesis of HCC through a physical interaction with nucleolin.

Silva et al. also showed that ZNF689 is highly expressed in HCC, but not in corresponding non-cancerous tissues [10]. They also remarked that targeting ZNF689 with anti-HCC drugs may be relatively safe because its expression is weak or absent in normal adult human tissues, except for the testis and placenta. Our preliminary study indicates that the expression of ZNF689 is not limited to HCC, but is also detected in a broad range of established cancer cell lines, such as human fibrosarcoma HT1080, cervical carcinoma cell line HeLa, and breast cancer cell line MCF7. In contrast, and consistent with previous observations, qPCR analysis showed that the expression of ZNF689 is extremely low in untransformed cells such as primary human hepatocytes, keratinocytes, and human umbilical vein endothelial cells (HUVEC) (data not shown). Therefore, ZNF689-mediated anti-apoptotic effects may have a more general role in the development of a wide variety of cancers.

In conclusion, we unveiled the anti-apoptotic mechanism of ZNF689 and propose that HCC cells that express ZNF689 at a high level can avoid cell death from chemotherapeutic drugs and proliferate. Our results suggest that siRNA against ZNF689 could be a crucial treatment for HCC, especially in the context of 5-FU-based combination chemotherapy. Further characterization of ZNF689 focusing on the apoptotic signaling pathway in HCC would improve understanding of proliferation and resistance to anticancer agents acquired by normal hepatocytes.

Supplementary materials related to this article can be found online at doi:10.1016/j.yexcr.2011.05.012.

Conflict of interest

The authors declare no conflict of interest.

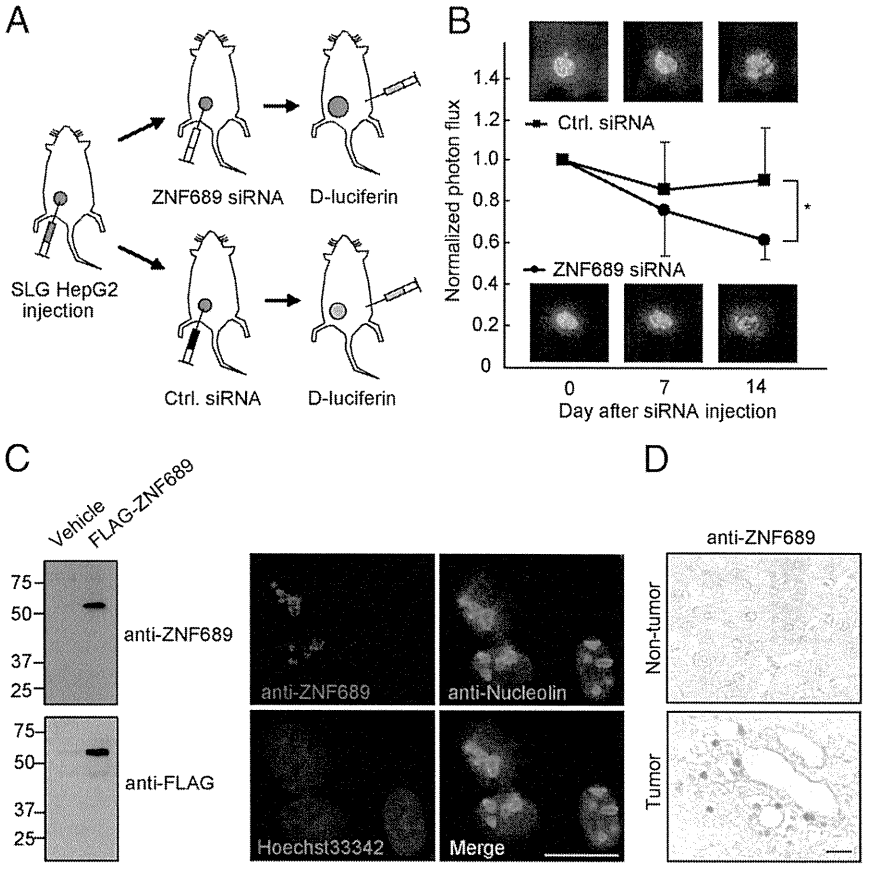

Fig. 6 – Physiological role of ZNF689 in HCC-transplanted mice and human hepatocellular carcinoma surgical specimens. A. Diagram of the seeding experiment. Luciferase-expressing liver cancer cells (SLG-HepG2) were subcutaneously injected into nude mice. When tumors were observed by bioluminescence imaging, siRNA was injected into the tumor at a final concentration of 10 nM. B. Luminescent signals of seeded tumors at the indicated time points. Color-range indicates photon flux. n = 4–5. The asterisk indicates $p < 0.05$. C. ZNF689 localized in the nucleolus. Antibody against the linker region of ZNF689 was used for Western blot analysis and immunocytochemistry. The antibody detected exogenous FLAG-tagged ZNF689 as a single band in Huh7 cells (left panels). Nucleoli and nuclei were detected by anti-Nucleolin antibody and Hoechst33342, respectively. Scale bar, 10 μm. D. Detection of the ZNF689 protein in the nucleus of hepatocellular surgical specimens. Scale bar, 10 μm.

Acknowledgments

We thank Dr. Licht (Northwestern University Feinberg School of Medicine) for kindly providing the Bak promoter-luciferase reporter plasmid and Dr. Tanimoto (Ehime University Graduate School of Medicine) for the staining of human liver specimen. We also thank members of Higashiyama and Onji laboratories for technical assistance, helpful comments, and discussion. This work was supported by Grant-in-Aid for Scientific Research (no. 17014068 and no. 20390082) to S. Higashiyama, and also supported in part by Program for Enhancing Systematic Education in Graduate School, from the Ministry of Education, Culture, Sports, Science, and Technology, Japan.

REFERENCES

[1] A.S. Befeler, A.M. Di Bisceglie, Hepatocellular carcinoma: diagnosis and treatment, Gastroenterology 122 (2002) 1609–1619.

[2] J. Bruix, M. Sherman, Management of hepatocellular carcinoma, Hepatology 42 (2005) 1208–1236.

[3] M.A. Avila, C. Berasain, B. Sangro, J. Prieto, New therapies for hepatocellular carcinoma, Oncogene 25 (2006) 3866–3884.

[4] C. Berasain, J. Castillo, M.J. Perugorria, M.U. Latasa, J. Prieto, M.A. Avila, Inflammation and liver cancer: new molecular links, Ann. N. Y. Acad. Sci. 1155 (2009) 206–221.

[5] Y. Inui, S. Higashiyama, S. Kawata, S. Tamura, J. Miyagawa, N. Taniguchi, Y. Matsuzawa, Expression of heparin-binding epidermal growth factor in human hepatocellular carcinoma, Gastroenterology 107 (1994) 1799–1804.

[6] D. Nanba, A. Mammoto, K. Hashimoto, S. Higashiyama, Proteolytic release of the carboxy-terminal fragment of proHB-EGF causes nuclear export of PLZF, J. Cell Biol. 163 (2003) 489–502.

[7] M. Hieda, M. Isokane, M. Koizumi, C. Higashi, T. Tachibana, M. Shudou, T. Taguchi, Y. Hieda, S. Higashiyama, Membrane-anchored growth factor, HB-EGF, on the cell surface targeted to the inner nuclear membrane, J. Cell Biol. 180 (2008) 763–769.

[8] Y. Kinugasa, M. Hieda, M. Hori, S. Higashiyama, The carboxyl-terminal fragment of pro-HB-EGF reverses Bcl6-mediated gene repression, J. Biol. Chem. 282 (2007) 14797–14806.

[9] W.H. Su, C.C. Chao, S.H. Yeh, D.S. Chen, P.J. Chen, Y.S. Jou, D.B. Onco, HCC: an integrated oncogenomic database of hepatocellular carcinoma revealed aberrant cancer target genes and loci, Nucleic Acids Res. 35 (2007) D727–D731.
[10] F.P. Silva, R. Hamamoto, Y. Furukawa, Y. Nakamura, TIPUH1 encodes a novel KRAB zinc-finger protein highly expressed in human hepatocellular carcinomas, Oncogene 25 (2006) 5063–5070.
[11] G. Kroemer, S.J. Martin, Caspase-independent cell death, Nat. Med. 11 (2005) 725–730.
[12] H. Puthalakath, A. Strasser, Keeping killers on a tight leash: transcriptional and post-translational control of the pro-apoptotic activity of BH3-only proteins, Cell Death Differ. 9 (2002) 505–512.
[13] D.J. Morrison, M.A. English, J.D. Licht, WT1 induces apoptosis through transcriptional regulation of the proapoptotic Bcl-2 family member Bak, Cancer Res. 65 (2005) 8174–8182.
[14] Y. Deng, X. Ren, L. Yang, Y. Lin, X. Wu, A JNK-dependent pathway is required for TNFalpha-induced apoptosis, Cell 115 (2003) 61–70.
[15] D.C. Schultz, J.R. Friedman, F.J. Rauscher III, Targeting histone deacetylase complexes via KRAB-zinc finger proteins: the PHD and bromodomains of KAP-1 form a cooperative unit that recruits a novel isoform of the Mi-2alpha subunit of NuRD, Genes Dev. 15 (2001) 428–443.
[16] R. Reed, K. Magni, A new view of mRNA export: separating the wheat from the chaff, Nat. Cell Biol. 3 (2001) E201–E204.
[17] M. Srivastava, H.B. Pollard, Molecular dissection of nucleolin's role in growth and cell proliferation: new insights, FASEB J. 13 (1999) 1911–1922.
[18] T. Lindsten, A.J. Ross, A. King, W.X. Zong, J.C. Rathmell, H.A. Shiels, E. Ulrich, K.G. Waymire, P. Mahar, K. Frauwirth, Y. Chen, M. Wei, V.M. Eng, D.M. Adelman, M.C. Simon, A. Ma, J.A. Golden, G. Evan, S.J. Korsmeyer, G.R. MacGregor, C.B. Thompson, The combined functions of proapoptotic Bcl-2 family members bak and bax are essential for normal development of multiple tissues, Mol. Cell 6 (2000) 1389–1399.
[19] M.C. Wei, W.X. Zong, E.H. Cheng, T. Lindsten, V. Panoutsakopoulou, A.J. Ross, K.A. Roth, G.R. MacGregor, C.B. Thompson, S.J. Korsmeyer, Proapoptotic BAX and BAK: a requisite gateway to mitochondrial dysfunction and death, Science 292 (2001) 727–730.
[20] R. Urrutia, KRAB-containing zinc-finger repressor proteins, Genome Biol. 4 (2003) 231.
[21] M.D. Esposti, The roles of Bid, Apoptosis 7 (2002) 433–440.
[22] L.P. Billen, A. Shamas-Din, D.W. Andrews, Bid: a Bax-like BH3 protein, Oncogene 27 (Suppl. 1) (2008) S93–S104.
[23] L. Montanaro, D. Trere, M. Derenzini, Nucleolus, ribosomes, and cancer, Am. J. Pathol. 173 (2008) 301–310.
[24] M. Derenzini, D. Trere, F. Oliveri, E. David, P. Colombatto, F. Bonino, M.R. Brunetto, Is high AgNOR quantity in hepatocytes associated with increased risk of hepatocellular carcinoma in chronic liver disease? J. Clin. Pathol. 46 (1993) 727–729.
[25] D. Trere, M. Borzio, A. Morabito, F. Borzio, M. Roncalli, M. Derenzini, Nucleolar hypertrophy correlates with hepatocellular carcinoma development in cirrhosis due to HBV infection, Hepatology 37 (2003) 72–78.
[26] A. Arabi, S. Wu, K. Ridderstrale, H. Bierhoff, C. Shiue, K. Fatyol, S. Fahlen, P. Hydbring, O. Soderberg, I. Grummt, L.G. Larsson, A.P. Wright, c-Myc associates with ribosomal DNA and activates RNA polymerase I transcription, Nat. Cell Biol. 7 (2005) 303–310.
[27] C. Grandori, N. Gomez-Roman, Z.A. Felton-Edkins, C. Ngouenet, D.A. Galloway, R.N. Eisenman, R.J. White, c-Myc binds to human ribosomal DNA and stimulates transcription of rRNA genes by RNA polymerase I, Nat. Cell Biol. 7 (2005) 311–318.

Splenic Elasticity Measured with Real-time Tissue Elastography Is a Marker of Portal Hypertension[1]

Masashi Hirooka, MD, PhD
Hironori Ochi, MD
Yohei Koizumi, MD, PhD
Yoshiyasu Kisaka, MD, PhD
Masanori Abe, MD, PhD
Yoshio Ikeda, MD, PhD
Bunzo Matsuura, MD, PhD
Yoichi Hiasa, MD, PhD
Morikazu Onji, MD, PhD

Purpose: To prospectively correlate spleen elasticity and degree of portal hypertension estimated with the hepatic venous pressure gradient (HVPG) and to evaluate splenic elasticity as a predictor of gastroesophageal varices.

Materials and Methods: The institutional review board approved this study, and patients provided written informed consent. In a pilot study of 60 patients with chronic liver damage, the authors measured liver and spleen elasticity with real-time tissue elastography (RTE), obtained serum markers related to fibrosis, examined hepatic and splenic blood flow with duplex Doppler ultrasonography, estimated HVPG, and performed upper gastrointestinal endoscopy. Then, with use of thresholds determined in the pilot study, the authors conducted a validation trial with another 210 patients, performing all studies except the measurement of HPVG. The relationship between HVPG and the other parameters was analyzed. Sensitivity, specificity, positive predictive value (PPV), and negative predictive value (NPV) in the diagnosis of gastroesophageal varices were calculated by using cutoff values obtained from receiver operating characteristic curves.

Results: Among the parameters associated with HVPG, correlation was closest with splenic elasticity ($R = 0.854$, $P < .0001$). When 8.24 was selected as the cutoff of splenic elasticity for predicting HVPG of more than 10 mm Hg, the accuracy of diagnosing gastroesophageal varix was 90% (sensitivity, 96%; specificity, 85%; PPV, 83%; NPV, 97%). The results of the validation trial showed that the 8.24 cutoff for splenic elasticity was associated with a diagnostic accuracy of 94.8% (sensitivity, 98%; specificity, 93.8%; PPV, 82.1%; NPV, 99.4%) for gastroesophageal varices.

Conclusion: Splenic elasticity determined with RTE is the most closely associated parameter for evaluating HVPG and is useful as a clinical marker of portal hypertension and a predictive marker of gastroesophageal varices.

[1] From the Department of Gastroenterology and Metabology, Ehime University Graduate School of Medicine, Shitsukawa, Toon, Ehime 791-0295, Japan. Received January 24, 2011; revision requested March 12; revision received June 5; accepted June 29; final version accepted July 14. Y.H. supported in part by a Grant-in-Aid for Scientific Research (JSPS KAKENHI 21590848) from the Japanese Ministry of Education, Culture, Sports, Science and Technology and a Grant-in-Aid for Scientific Research and Development from the Japanese Ministry of Health, Labour and Welfare.
Address correspondence to Y.H. (e-mail: *hiasa@m.ehime-u.ac.jp*).

The architectural distortion of liver cirrhosis leads to increased intrahepatic resistance, which in turn elevates portal venous pressure (1). Elevated portal venous pressure is related not only to the occurrence of an esophageal varix but also to liver failure (2), ascites (3), and bacterial translocation—including spontaneous bacterial peritonitis (4). The accurate identification of portal venous pressure is clinically important for estimating patient status and prognosis.

However, portal venous pressure can only be directly measured by using invasive techniques such as direct portal venography or direct splenic puncture. The hepatic venous pressure gradient (HVPG) is the currently accepted reference standard with which to evaluate portal hypertension (5). However, this is limited in clinical application because it is invasive. Moreover, HVPG cannot provide an accurate estimate of pressure in the portal vein. Thus, a parameter that can substitute for HVPG is desirable (6). Some investigators have indicated that measurement of hepatic elasticity could be a noninvasive method for determining portal venous pressure and may be useful for screening patients for conventional examinations including upper gastrointestinal endoscopy and hemodynamic studies (7). Moreover, the ability to noninvasively measure organ elasticity with ultrasonographic (US) or magnetic resonance (MR) elastography has provided the opportunity to investigate whether splenic elasticity is related to portal pressure (8). Recent preliminary results from a few healthy volunteers and patients with chronic liver disease have shown that splenic stiffness might be a better indicator of portal pressure than of hepatic elasticity (8). Elevated portal venous pressure causes histologic changes in the spleen (9–12). Doppler US (13) and transient elastography (14,15) might help predict the presence of clinically important portal hypertension, but these modalities cannot help accurately predict HVPG. The value of spleen elasticity determined with MR elastography in the prediction of esophageal varices has been reported (8). Spleen elasticity should be closely related to portal venous pressure because histologic changes in the spleen would be directly caused by portal hypertension. US-based real-time tissue elastography (RTE) can also help measure spleen elasticity. Measurements of spleen stiffness are not comparable among transient elastography, MR elastography, and RTE because RTE is a qualitative method of imaging elasticity and MR elastography and tissue elastography are quantitative. RTE, however, is an easier, more economical, and faster approach that does not require a specific dedicated system.

We established that RTE is useful for assessing liver fibrosis in patients with chronic hepatitis C (16). If splenic elasticity closely correlates with HVPG, it could serve as a predictive marker of a gastroesophageal varix before gastrointestinal endoscopy is performed.

We aimed to prospectively correlate spleen elasticity with the degree of portal hypertension estimated with the HVPG and to evaluate splenic elasticity as a predictor of gastroesophageal varices.

Advances in Knowledge

- The correlation between splenic elasticity evaluated with real-time tissue elastography and the degree of portal hypertension estimated with the hepatic venous pressure gradient (HVPG) is high ($R = 0.855$; 95% confidence interval: 0.767, 0.911; $P < .0001$).
- When 8.24 was used as the cutoff of splenic elasticity for predicting HVPG of more than 10 mm Hg, the accuracy of diagnosing gastroesophageal varix was 90%; sensitivity, 96%; specificity, 85%; positive predictive value, 83%; and negative predictive value, 97%.

Implication for Patient Care

- Splenic elasticity can be used as an accurate noninvasive predictor of the severity of portal hypertension and varices; in addition, it may help identify patients who are at risk for gastrointestinal bleeding.

Materials and Methods

Patients

Our institutional ethics committee approved all study protocols, and patients provided written informed consent. We initially enrolled 277 consecutive patients with chronic liver disease who underwent RTE between January 2009 and February 2010. Exclusion criteria were obesity (body mass index >25) that prevented splenic US measurements of elasticity ($n = 6$) and portal tumor thrombus associated with hepatocellular carcinoma that was not confirmed as being chronic ($n = 1$). The final number of participating patients was 270 (Fig 1). In the pilot portion of the study, liver and spleen elasticity were measured in 60 patients between January and May 2009. We also measured HVPG in these patients, and they agreed to undergo upper gastrointestinal

Published online before print
10.1148/radiol.11110156 **Content codes:** GI US

Radiology 2011; 261:960–968

Abbreviations:
ALT = alanine aminotransferase
APRI = aspartate aminotransferase–to–platelet ratio index
AST = aspartate aminotransferase
AUC = area under the ROC curve
CI = confidence interval
HVPG = hepatic venous pressure gradient
NPV = negative predictive value
PPV = positive predictive value
RHA = right hepatic artery
ROC = receiver operating characteristic
RPV = right portal vein
RTE = real-time tissue elastography

Author contributions:
Guarantors of integrity of entire study, M.H., H.O., Y. Koizumi, Y.H., M.O.; study concepts/study design or data acquisition or data analysis/interpretation, all authors; manuscript drafting or manuscript revision for important intellectual content, all authors; manuscript final version approval, all authors; literature research, M.H., H.O., Y. Koizumi, Y. Kisaka, Y.H.; clinical studies, all authors; statistical analysis, M.H., H.O., Y. Koizumi, Y.H.; and manuscript editing, M.H., Y.H., M.O.

Potential conflicts of interest are listed at the end of this article.

Figure 1

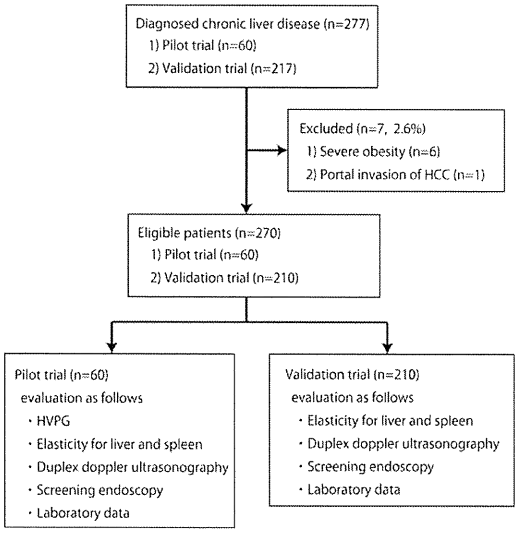

Figure 1: Flow chart of trial participants.

endoscopy. Subsequently, 210 patients participated in the validation trial, in which all studies included in the pilot study except for the measurement of HVPG were performed between June 2009 and February 2010.

Observers

Two hepatologists (M.H. and Y. Koizumi, with 13 and 6 years of experience, respectively) performed Doppler US and RTE. Both of these investigators had performed more than 100 liver and splenic stiffness evaluations before starting this study. Two other hepatologists (Y. Kisaka and H.O., with 10 and 4 years of experience, respectively) performed venography. They had previously measured HVPG in another 50 patients.

Measurements of Liver and Splenic Elasticity

Hepatic and splenic elasticity were measured by using RTE (EUB-7500; Hitachi Medical Systems, Tokyo, Japan) with a linear probe (central frequency, 5.5 MHz; EUP-L52, Hitachi Medical Systems) in B mode to visualize the liver and spleen and then in elastography mode (Fig 2). Regions of interest were simultaneously placed on small intrahepatic veins and hepatic parenchyma, and signals were evaluated. We then calculated the elastic ratio (proportion of small veins to that of hepatic or splenic parenchyma). The area of the regions of interest placed on both the liver and the spleen parenchyma was within 2 × 1 cm (long distance: mean ± standard deviation = 1.90 cm ± 0.12, range = 1.5–2 cm; short distance: mean = 0.90 cm ± 0.11, range = 0.6–1 cm). The size of the region of interest in the small vessels was usually within 0.3 × 0.5 cm (long distance: mean = 0.44 cm ± 0.07, range = 0.3–0.5 cm; short distance: mean = 0.28 cm ± 0.01, range = 0.2–0.3 cm). A higher elastic ratio is indicative of more hepatic and splenic elasticity. The means of five measurements were calculated as described (16).

Measurements from Doppler US

The patients fasted overnight and refrained from smoking cigarettes before undergoing five repeated Doppler US measurements with a 3.5-MHz probe (EUB-7500, Hitachi Medical Systems), as previously described (17). The Doppler sample gate was set at 4–5 mm for the portal vein and 2–3 mm from the arterial side. The angle was always less than 60°. The Doppler sampling cursor was placed in the middle of the portal vein with a width that was about half that of the lumen. Maximal blood velocity in the right portal vein (RPV) and right hepatic artery (RHA) were calculated from fast Fourier transformation values. The RHA/RPV ratio was calculated by dividing the maximal blood velocity of the RHA by that of the RPV (17). Maximal velocity and the diameter of the major portal trunk were also measured to calculate the congestion index of the portal vein by dividing its cross-sectional area by the blood flow velocity within it as described previously (18). Peak systolic velocity and end diastolic velocity were measured, and the splenic resistive index ([peak systolic velocity − end diastolic velocity]/peak systolic velocity) and pulsatility index ([peak systolic velocity − end diastolic velocity]/mean velocity) were determined. The resistive and pulsatility indexes of the splenic artery with the sampling cursor placed near the splenic hilum were measured by using the formulas described earlier.

Measurements of HVPG

The right hepatic vein was catheterized through the right femoral vein, and pressure in both the wedged and free position was measured by using a 5-F balloon-tipped catheter. The HVPG was calculated by subtracting the free hepatic venous pressure from the wedged venous pressure.

Clinical Data Collection

Basic demographic data, including age, sex, and cause of liver disease, were obtained from all patients. In addition, blood cell counts, biochemical data, coagulation profiles, and serologic data were obtained before performing US, upper gastrointestinal endoscopy, and measurement of HVPG. All examinations were performed within 1 week of each other. The functional grade of cirrhosis was determined with the Child-Pugh scoring system. Serum fibrosis markers, as well as the aspartate aminotransferase (AST)-to-alanine aminotransferase (ALT) ratio (19), the AST-to-platelet ratio index (APRI) (20), and the FIB-4

index (21) were calculated. The APRI was calculated by using the following formula: [(AST/reference AST) × 100]/platelet count. FIB-4 is a simple index for diagnosing hepatic fibrosis and is based on four parameters. The FIB-4 index was calculated as follows: [age (in years) × AST (in units per liter)]/[platelet count (in 10^{10}/L)] × [ALT (in units per liter)½]. Volumetric measurements of the spleen were automatically obtained from computed tomographic (CT) scans by using a workstation (Virtual Place Advance; AZE, Tokyo, Japan) (22). From the CT scans, we defined a huge shunt as one in which the diameter of the collateral vessels was greater than 10 mm.

Statistical Analysis

Results are expressed as means ± standard deviations. Data were analyzed by using the Student *t* test for unpaired data and the χ^2 test and Fisher exact test as appropriate. The relationship between HVPG and the other parameters was analyzed with the Pearson product-moment correlation coefficient. Receiver operating characteristic (ROC) curves were constructed, and the area under the ROC curve (AUC) was calculated by using the trapezoidal rule. Optimal cutoff values for liver stiffness were selected to maximize sensitivity, specificity, and diagnostic accuracy. Sensitivity, specificity, positive predictive value (PPV), and negative predictive value (NPV) were calculated by using cutoffs obtained from the ROC curves. The correlation between two variables was calculated by using the Pearson product-moment correlation coefficient. Univariate and multivariate logistic regression was performed with the Wald test. Multivariate logistic regression models included parameters that significantly differed in univariate analysis between an HVPG of less than or more than 10 mm Hg (splenic elasticity, hepatic elasticity, RHA/RPV ratio, platelet count) and an HVPG of less than or more than 12 mm Hg (splenic elasticity, hepatic elasticity, RHA/RPV ratio, platelet count, albumin level, prothrombin activity, FIB-4 index, and APRI). All data were analyzed with software (JMP, version 8; SAS Institute Japan, Tokyo, Japan).

Figure 2

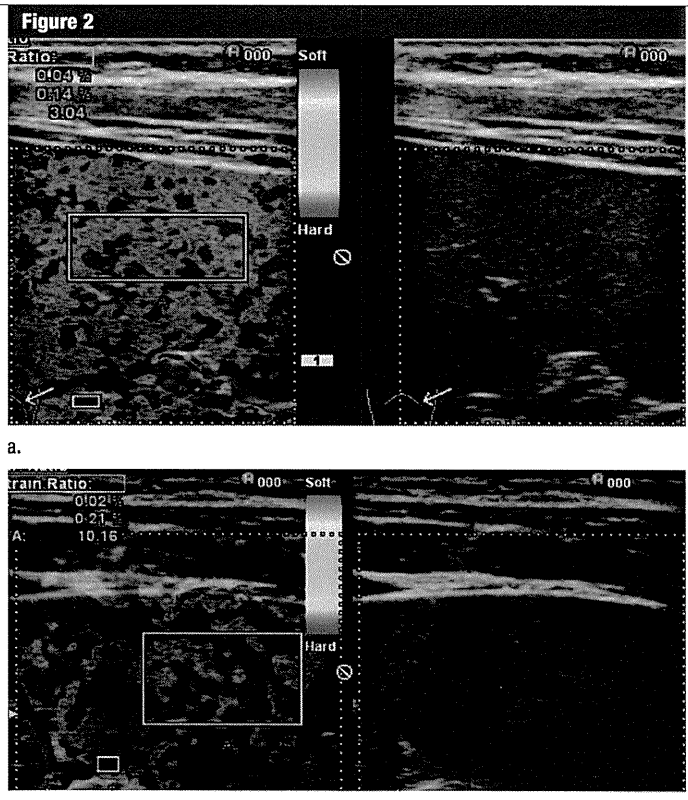

Figure 2: Splenic RTE images from patients with high and low HVPG. Image on right is B-mode image; image on left is color-coded elastography image overlaid on B-mode image. Rectangular boxes are regions of interest selected for splenic parenchyma (large box) and small vessel (small box). **(a)** Images in a 65-year-old man with hepatitis C–related liver cirrhosis (Child-Pugh class A) and without gastroesophageal varices. HVPG was low (6.76 mm Hg). Splenic and hepatic elastic ratios were 3.12 and 3.21, respectively. **(b)** Images in a 48-year-old man with hepatitis B–related liver cirrhosis (Child-Pugh class B) and gastroesophageal varices. HVPG was high (24.12 mm Hg). Splenic and hepatic elastic ratios were 10.10 and 3.41, respectively.

Results

Patient Characteristics

The characteristics of the patients in the training and validation sets did not significantly differ except for rates of varices, which were present in 26 of the 60 patients (43%) in the training set and 47 of the 210 (22%) in the validation set (P = .0049) (Table 1).

Parameters Associated with HVPG

Hepatic elasticity, splenic elasticity, RHA/RPV ratio, platelet count, FIB-4 index, and congestion index showed a significant correlation with HVPG (hepatic elasticity: r = 0.510, 95% confidence interval [CI] = 0.294, 0.676; splenic elasticity: r = 0.854, 95% CI = 0.767, 0.911; RHA/RPV ratio: r = 0.401, 95% CI = 0.164, 0.594; platelet count: r = 0.446, 95% CI = 0.217, 0.629; APRI: r = 0.255, 95% CI = 0.001, 0.478; FIB-4 index: r = 0.335, 95% CI = 0.089, 0.543; congestion index: r = 0.594,

Table 1

Patient Characteristics

Characteristic	Training Set	Validation Set	*P* Value
Age (y)*	68.0 ± 8.9 (35–89)	62.1 ± 12.7 (22–89)	.092
Men	67.4 ± 7.9 (54–89)	62.2 ± 12.6 (25–89)	.475†
Women	69.1 ± 10.5 (35–80)	62.0 ± 12.8 (22–84)	.920‡
M:F ratio	39:21	113:97	.138
Cause of liver damage§			
HBV	11	34	.079
HCV	43	131	
Alcohol	4	16	
NAFLD	1	17	
PBC	1	12	
Noncirrhosis	12		
Cirrhosis	48		
Child-Pugh class			
A (without cirrhosis)	46	161	.087
B	8	28	
C	6	21	
Esophageal varices			
Present	26	47	.0049
Absent	34	143	

Note—Except where indicated, data are numbers of patients.

* Data are means ± standard deviations, with ranges in parentheses.

† *P* value between men and women in the training set.

‡ *P* value between men and women in the validation set.

§ HBV = hepatitis B virus, HCV = hepatitis C virus, NAFLD = nonalcoholic fatty liver disease, PBC = primary biliary cirrhosis.

Table 2

Parameters Associated with HVPG in the Training Set

Parameter*	Mean ± SD†	*r* Value	95% CI
HVPG (mm Hg)	9.5 ± 6.1	NA‡	...
Hepatic elasticity	3.8 ± 0.77	0.510	0.294, 0.676
Splenic elasticity	7.6 ± 3.2	0.854	0.767, 0.911
RHA/RPV ratio	3.3 ± 1.0	0.401	0.164, 0.594
Spleen volume (cm^3)	299.5 ± 183.9	0.232	−0.023, 0.459
Platelet count ($\times 10^{10}$/L)	11.1 ± 6.4	0.446	0.217, 0.629
HOMA-IR	4.6 ± 3.0	0.097	−0.160, 0.343
AST/ALT ratio	1.5 ± 0.51	0.128	−0.13, 0.370
APRI	0.75 ± 0.95	0.255	0.001, 0.478
FIB-4 index	7.6 ± 7.3	0.335	0.089, 0.543
Congestion index	0.080 ± 0.061	0.594	0.401, 0.737
Splenic artery velocity (cm/sec)	55.9 ± 15.0	0.047	−0.209, 0.297
Splenic artery PI	1.48 ± 0.38	0.062	−0.195, 0.311
Splenic artery RI	0.68 ± 0.20	0.216	−0.040, 0.446

* HOMA-IR = homeostasis model assessment of insulin resistance, PI = pulsatility index, RI = resistive index.

† SD = standard deviation.

‡ NA = not applicable.

95% CI = 0.401, 0.737) (Table 2). None of the other measured parameters (ie, spleen volume, homeostasis model assessment of insulin resistance, AST/ALT ratio, peak velocity of the splenic artery, pulsatility index of the splenic artery, or resistive index of the splenic artery) showed significant correlation with HVPG. Although both splenic and hepatic elasticity were linearly correlated with HVPG, the *r* value was higher for splenic than for hepatic elasticity (Fig 3, Table 2). Only four patients in our cohort had vascular abnormalities of at least 10 mm nourished by collateral vessels and shunts, and these were located in the lower part of the correlation line (Fig 3a).

Diagnostic Accuracy for Predicting Elevated HVPG and the Presence of Gastroesophageal Varices

HVPG was elevated by more than 10 and 12 mm Hg in 28 and 19 patients, respectively. Hepatic elasticity (AUC, 0.832; 95% CI: 0.714, 0.917; $P = .0042$), splenic elasticity (AUC, 0.978; 95% CI: 0.902, 0.999; $P < .0001$), RHA/RPV ratio (AUC, 0.748; 95% CI: 0.619, 0.851; $P < .0001$), platelet count (AUC, 0.809; 95% CI: 0.688, 0.900; $P = .0040$), and congestion index (AUC, 0.740; 95% CI: 0.713, 0.916; $P = .0019$) were significant factors for predicting HVPG elevation of more than 10 mm Hg (Table 3). Among these parameters, splenic elasticity was the most accurate predictive factor for HVPG elevation (>10 mm Hg). Significantly predictive parameters in the univariate analysis (splenic elasticity, hepatic elasticity, RHA/RPV ratio, and platelet count) were entered into a multivariate logistic regression model to predict elevation of HVPG of more than 10 mm Hg (Table 4). Only splenic elasticity was selected as a significant factor (odds ratio, 9.070; 95% CI: 2.277, 134.290; $P = .020$).

The results for predicting an HVPG elevation of more than 12 mm Hg were similar. When analyzed with use of ROC curves, hepatic elasticity (AUC, 0.781; 95% CI: 0.656, 0.878; $P = .0004$), splenic elasticity (AUC, 0.948; 95% CI: 0.859, 0.989; $P < .0001$), platelet count (AUC, 0.798; 95% CI: 0.675, 0.891; $P = .0078$), and congestion index (AUC, 0.806; 95% CI: 0.684, 0.897; $P = .0001$) were also significantly better for predicting HVPG elevation of more than 12 mm Hg (Table 3). In the multivariate analysis of the parameters that

significantly differed in the univariate analysis between HVPG of more than or less than 12 mm Hg, splenic elasticity was the only significantly predictive parameter (odds ratio, 17.708; 95% CI: 2.591, 765.094; $P = .040$) (Table 5).

The diagnostic accuracy of cutoff values for splenic elasticity in predicting the presence of gastroesophageal varices was 90% (sensitivity, 96%; specificity, 85%; PPV, 83%; NPV, 97%) (Table 6) with a cutoff value of 8.24 for HVPG of more than 10 mm Hg selected from the ROC curves in the training set and 78% (sensitivity, 54%; specificity, 97%; PPV, 93%; NPV, 73%) (Table 6) with a cutoff value of 9.99 selected as the splenic elasticity required to predict an elevated HVPG of more than 12 mm Hg. We could not measure HVPG in all patients in the validation set. Thus, the diagnostic accuracy of gastroesophageal varices was analyzed by using the corresponding splenic elasticity for HVPG from the ROC curves (HVPG of 10 and 12 mm Hg corresponded to cutoff values for splenic elasticity of 8.24 and 9.99, respectively). The diagnostic accuracy of the same cutoff values in patients with HVPG of more than 10 and 12 mm Hg in the validation set was 94.8% (sensitivity, 98%; specificity, 93.8%; PPV, 82%; NPV, 99.4%) and 82.9% (sensitivity, 26%; specificity, 99.4%, PPV, 92%; NPV, 82.2%), respectively (Table 6). When splenic elasticity was set at the cutoff (8.24 for HVPG of 10 mm Hg; 9.99 for HVPG of 12 mm Hg), sensitivity, specificity, PPV, NPV, and diagnostic accuracy were high in both the training and validation sets. The validation set indicated that a cutoff value of 9.99 for splenic elasticity would be highly accurate in the prediction of a gastroesophageal varix.

Figure 3

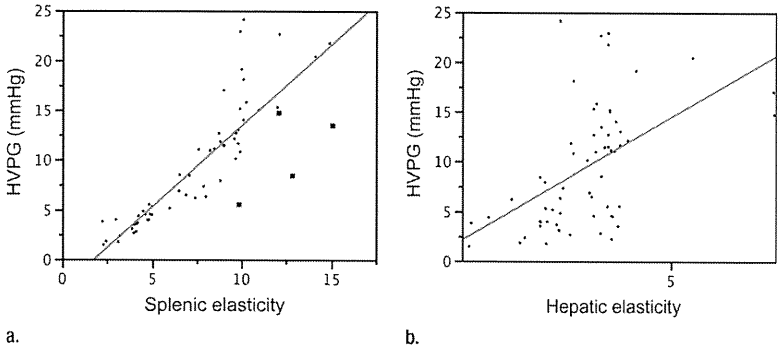

Figure 3: **(a)** Scatterplot shows correlation between splenic elastic ratio and HVPG among patients in training set. Splenic elasticity and HVPG show significant linear correlation ($R = 0.85$, $P < .0001$). Square data points indicate patients with vascular abnormalities of at least 10 mm nourished by collateral vessels and shunts. **(b)** Scatterplot shows correlation between hepatic elasticity and HVPG ($R = 0.51$, $P < .0001$).

Table 3

Comparison of AUCs for Predicting Elevated HVPG and the Presence of Gastroesophageal Varices in the Training Set

Parameter*	HVPG >10 mm Hg	HVPG >12 mm Hg	Varices
Hepatic elasticity	0.832 (0.714, 0.917)	0.781 (0.656, 0.878)	0.833 (0.714, 0.917)
Splenic elasticity	0.978 (0.902, 0.999)	0.948 (0.859, 0.989)	0.908 (0.873, 0.993)
RHA/RPV ratio	0.748 (0.619, 0.851)	0.743 (0.614, 0.847)	0.756 (0.628, 0.858)
Spleen volume	0.739 (0.609, 0.844)	0.681 (0.550, 0.797)	0.747 (0.619, 0.851)
Platelet count	0.809 (0.688, 0.900)	0.798 (0.675, 0.891)	0.811 (0.691, 0.801)
HOMA-IR	0.617 (0.568, 0.811)	0.613 (0.478, 0.736)	0.731 (0.601, 0.838)
AST/ALT ratio	0.573 (0.439, 0.700)	0.765 (0.498, 0.753)	0.545 (0.412, 0.674)
APRI	0.705 (0.621, 0.853)	0.746 (0.638, 0.865)	0.748 (0.620, 0.851)
FIB-4 index	0.778 (0.652, 0.875)	0.822 (0.702, 0.909)	0.766 (0.640, 0.866)
Congestion index	0.740 (0.713, 0.916)	0.806 (0.684, 0.897)	0.852 (0.738, 0.931)
Splenic artery velocity	0.474 (0.343, 0.607)	0.524 (0.390, 0.653)	0.477 (0.390, 0.653)
Splenic artery PI	0.575 (0.441, 0.703)	0.497 (0.370, 0.634)	0.611 (0.478, 0.736)
Splenic artery RI	0.629 (0.495, 0.751)	0.611 (0.476, 0.734)	0.635 (0.501, 0.756)

Note.—Data are AUCs. Numbers in parentheses are 95% CIs.

* HOMA-IR = homeostasis model assessment of insulin resistance, PI = pulsatility index, RI = resistive index.

Discussion

Splenic elasticity has a close linear relationship with HVPG and can help predict the presence of esophageal varices in patients with chronic liver disease.

There are some possible explanations for why splenic elasticity is more closely associated with HVPG. Portal hypertension would initially and directly induce hypersplenism, which would increase spleen elasticity and be reflected as histologic changes in the spleen. Splenic elasticity is the result of portal hypertension, which develops as a result of hepatic elasticity that increases not only because of hepatic fibrosis but also as a result of structural and biologic changes that are related to portal hypertension (23,24). These include major angioarchitectural modifications involving neoangiogenesis and the presence of cell types undergoing active contraction in response to the intrahepatic predominance of vasoconstrictor stimuli (25,26). Portal hypertension will evoke hyperplasia among splenic histiocytes (9), arterial terminal lengthening (10), increased white pulp volume (11), and even fibrosis between splenic trabeculae (12). These changes result in portal hypertension and, thus, increased splenic elasticity.

Another reason why the spleen is more elastic than the liver could be the anatomic shape of these organs. Hepatic